HOKKAIDO UNIVERSITY

Title	End bearing capacity of a single incompletely end-supported pile based on the rigid plastic finite element method with non-linear strength property against confining stress
Author(s)	Tamboura, Hamidou Hamadoum; Isobe, Koichi; Ohtsuka, Satoru
Citation	Soils and Foundations, 62(4), 101182 https://doi.org/10.1016/j.sandf.2022.101182
Issue Date	2022-08
Doc URL	http://hdl.handle.net/2115/86655
Rights(URL)	http://creativecommons.org/licenses/by-nc-nd/4.0/
Type	article
File Information	1-s2.0-S0038080622000907-main.pdf

Technical Paper

End bearing capacity of a single incompletely end-supported pile based on the rigid plastic finite element method with non-linear strength property against confining stress

Hamidou Hamadoum Tamboura [a],*, Koichi Isobe [b], Satoru Ohtsuka [c]

[a] *Laboratory of Analytical Geomechanics, Division of Civil Engineering, Graduate School of Engineering, Hokkaido University, Kita 13, Nishi 8, Kita-Ku, Sapporo, Hokkaido 060-8628, Japan*
[b] *Laboratory of Analytical Geomechanics, Division of Civil Engineering, Graduate School of Engineering, Hokkaido University, Kita 13, Nishi 8, Kita-Ku, Sapporo, Hokkaido 060-8628, Japan*
[c] *Department of Civil and Environmental Engineering, Nagaoka University of Technology, 1603-1 Kamitomioka, Nagaoka, Niigata 940-2188, Japan*

Abstract

An Incompletely End Supported Pile (IESP) is a pile in a soft soil layer underlain by a hard soil layer that does not reach the bottom hard layer in practice. This study estimates the end bearing capacity of IESP by using an inhouse Rigid Plastic FEM code (RPFEM), considering shear strength non-linearity of soil against confining pressure, and soil-foundation interaction. The effect of the distance between the pile tip and the bottom hard soil layer (d/B) on the end-bearing capacity of IESP was mainly investigated for three types of soil: cohesive soils, cohesionless soils and intermediate soils. Also, the ratio (r) of the end bearing capacity of the pile when it reaches the bottom hard layer to that of the pile when the bottom layer has no influence was was considered. By considering the shear strength non-linearity, the end bearing capacity was accurately estimated. The estimations were consistent with previous analytical, experimental and numerical solutions. It is found that the end bearing capacity inversely decreases with the distance d/B and becomes constant around $d/B = 3$. Based on the results, a formula for estimating the end bearing capacity of IESP is proposed. Comparisons with methods in existing literature confirmed the reliability of the proposed equation.
© 2022 Production and hosting by Elsevier B.V. on behalf of The Japanese Geotechnical Society. This is an open access article under the CC BY-NC-ND license (http://creativecommons.org/licenses/by-nc-nd/4.0/).

Keywords: End bearing capacity; Incompletely end supported pile; Rigid plastic finite element method

1. Introduction

One of the reasons for the use of pile foundations in foundation engineering is to transfer loads to a deeper and more competent soil layer when the upper soil layers are weaker. However, when the soil layers are non-horizontal due to complex geologic formation, some pile tips may not reach the targeted stiffer bottom and end up in an upper soil layer. A schematic view of this phenomenon is shown in Fig. 1 with piles in a two-layered ground. The piles that reach the stiffer bottom layer are called End Supported Piles (ESP) and those that did not reach the stiffer bottom layer are referred to as Incompletely End Supported Piles (IESP). While the skin friction resistance of IESP might be the same as that of ESP, the end bearing capacity of IESP is reduced by the presence of the softer soil at the pile toe. The amount of reduction of the end bearing capacity of IESP depends on the
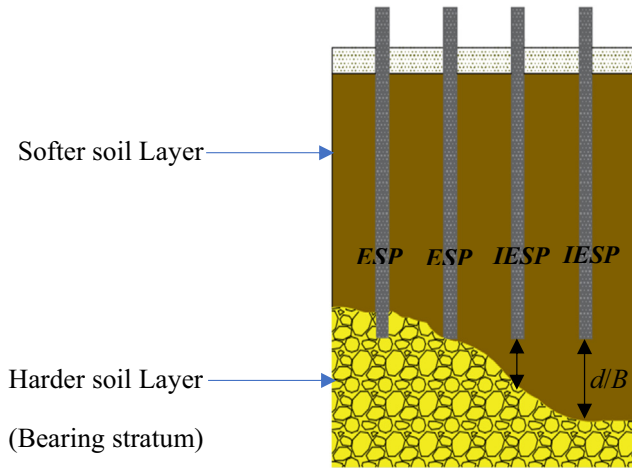
Fig. 1. IESP caused by a non-horizontal bearing stratum.

distance to the stiffer bottom layer. Hence, the main concern of this study is to determine the influence of the distance to the bottom layer on the end bearing capacity of IESP. The occurrence of IESP may cause the tilting of the structure it supports. Thus, IESP can threaten the integrity of the structure it supports and can cause the failure of structures, which can lead to fatalities and economic losses. Therefore, it is necessary to assess the end-bearing capacity of IESP appropriately to evaluate the stability and safety of the structure supported. While it is possible that the pile end-bearing capacity is affected by the presence of debris at the pile tip during driven and bored piles construction procedure, this is not considered in this study. That is, this study is limited to cases without debris at the pile tip.

The end bearing capacity of a pile is analogous to the bearing capacity of a shallow foundation with a very large depth of footing (Gunaratne, 2006). There are different solutions of the end bearing capacity of piles. Theoretical methods based on geotechnical considerations, such as the Prandtl's method (1921), Terzaghi's method (1943), Meyerhof's method (1963) and Vesic's method (1973), are often used to analyze the characteristics of pile end bearing capacity in uniform ground.

Theoretical and experimental studies have been conducted to propose formulas for end bearing capacity of driven and bored and cast in place piles. These include studies by Meyerhof (1976), Vesić (1977), Janbu (1976), Coyle and Castello (1981), Eslami and Fellenius (1995, 1997), Yasufuku and Hyde (1995), Yasufuku et al. (2001), and Veiskarami et al. (2011). None of these studies are directly applicable in the case of layered soil.

Experimental studies have been conducted to investigate the end bearing capacity of pile in layered ground. Houlsby et al. (1994) conducted an experimental study and proposed a method to calculate the pile end bearing capacity in layered soil. However, this does not apply to IESP. Ikeda et al. (2012) conducted laboratory loading tests of pile in layered sand and found that the end bearing

capacity decreases significantly when the pile moves away from the bottom hard layer. However, it did not propose any formula for the influence of the bottom layer on the end bearing capacity. Pholkainuwatra et al. (2022) conducted an experimental study of pile set-up of driven piles in Bangkok clay using seven piles with their pile tips varied between 8 and 21 m below ground level. The soil condition was found to change with depth from soft clay with 12 m of thickness passing by 6 m of medium clay to 4 m of stiff clay. However, they did not mention the effect of the layers on the bearing capacity or propose a formula to determine the effect.

Some researchers have used numerical analysis to investigate the end bearing capacity of IESP. Teramoto et al. (2015) conducted an FEM analysis to investigate the mechanical behaviors of Incompletely End-Supported Piles. They found that the gap between the pile tip and bottom layer influences the bearing capacity, but did not propose a formula. Hyodo et al. (2020) studied the end bearing capacity of IESP in sand using a three-dimensional elasto-plastic FEM analysis. They proposed a ratio of the degradation of the end bearing capacity of IESP when the pile tip moves away from the bottom layer. However, their proposed formula applied to sand only.

As mentioned above, there is no concrete solution for the end bearing capacity of piles in layered grounds that considers the effect of the distance to a bottom stiffer layer for all different types of soils. Such formulas, however, exist for a shallow foundations. For example, for c-φ soils, there are the formulas of Satyanarayana and Garg (1980), Azam and Wang (1991), Bowles (1996),... which consider the distance between the footing and the bottom layer. These formulas can be used to analyze the characteristics of pile end bearing capacity in a two-layered ground, according to Gunaratne (2006).

The main objective of this study is to investigate the influence of the bottom layer on the end bearing capacity of IESP. That is, the aim is to determine the extent of the decrease (degradation) in the end bearing capacity of IESP when the distance from the pile tip to the bottom layer increases. The two-dimensional Rigid Plastic FEM is used to consider the non-linear shear strength property against the confining pressure and soil-pile interaction. In addition, a formula of the end bearing capacity of IESP for all types of soils (cohesive soils, cohesionless soils and intermediate soils) is proposed based on the results, and the influence of the end bearing capacity ratio r is considered.

2. Some existing formulas of pile end bearing capacity

2.1. Theoretical formula of pile end bearing capacity

The ultimate end bearing capacity of a pile, q_{pult}, may be expressed by an equation similar to that of a footing as follows:

$$q_{\mathrm{pult}} = cN_{\mathrm{c}} + qN_{\mathrm{q}} + 0.5\gamma BN_{\gamma} \tag{1}$$

where B = diameter or width of the pile, q = overburden pressure, c = cohesion of soil, γ = unit weight of soil and N_c, N_q and N_γ are bearing capacity factors for deep foundations, which are different from those of shallow foundations.

Because the width B of the pile is relatively small, the third term $0.5\gamma B N_\gamma$ becomes insignificant in comparison with the second term qN_q and is dropped. Therefore Eq. (1) reduces to.

$$q_{pult} = cN_c + qN_q \qquad (2)$$

Vesić (1967) has revealed that the bearing capacity of a pile remains constant beyond a critical depth, and N_q depends on ϕ and D/B (where D = length of embedment, B = diameter or width of the pile).

Meyerhof (1976) proposed the critical depth ratio (D_c/B) in Fig. 2 for N_c and N_q. N_c and N_q increase with D_b/B and reach a maximum value at D_b/B equal to about 0.5 (D_c/B), where D_b is the actual thickness of the bearing stratum. In a homogeneous soil, D_b is equal to the embedded length of the pile (L); whereas, in layered soil, D_b is less than L.

Meyerhof prescribed a limiting value for q_{pult}. The expression sfor the limiting value, q_{pl} are:

$$\text{for dense sand} : q_{pl} = 50N_q\tan\phi\,(kN/m^2) \qquad (3)$$

$$\text{for loose sand} : q_{pl} = 25N_q\tan\phi\,(kN/m^2) \qquad (4)$$

The equation for tip resistance in sand may now be expressed as.

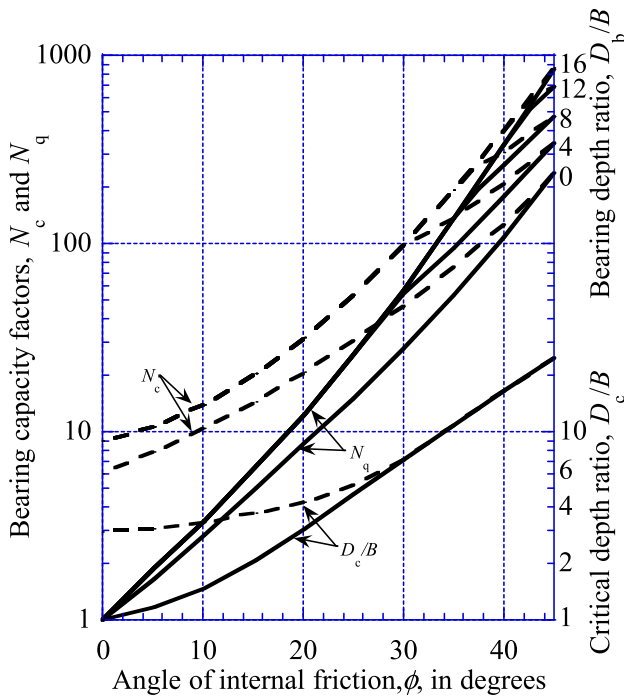$$q_{pult} = q'_0 N_q \leq q_{pl} \qquad (5)$$

Fig. 2. Bearing capacity factors and critical depth ratios for driven piles. (After Meyerhof (1976)).

where q'_0 = effective overburden pressure at the tip of the pile corresponding to D_c/B and N_q = bearing capacity factor (Fig. 2). Eq. (5) is applicable only for driven piles in sand. For bored cast-in-situ piles, the value of q_{pult} is to be reduced by one-third to one-half.

2.2. Theoretical formulas applicable to end bearing capacity of IESP

Hyodo et al. (2020) studied the end bearing capacity of IESP in sand using an elastoplastic FEM and proposed Eq. (6) below to estimate the end bearing capacity.

$$q_{unreached} = \alpha q_{base} + (1 - \alpha)q_{nobase} \qquad (6)$$

where $q_{unreached}$ is the pile end resistance of IESP, q_{base} is the pile end resistance of the completely end-supported pile, q_{nobase} is the pile end resistance of the pile with no lower hard layer, and α is the degradation factor which represents the incompleteness of the pile end support. An amelioration of the formula of Hyodo et al. (2020) is proposed in this study.

On the other hand, the empirical formulas of Satyanarayana and Garg (1980) and Azam and Wang (1991) can be used to analyze the end bearing capacity of IESP in c-ϕ soil.

Satyanarayana and Garg (1980) conducted a study to determine the ultimate bearing capacity of footings in a two-layered c-ϕ soil system. They suggested empirical equations to determine the average value of cohesion c_{av}, the average value of the angle of internal friction ϕ_{av}, and equivalent significant depth H_2 for a layered soil system. With such strength parameters, they proposed a simplified bearing-capacity theory for shallow foundations in c-ϕ soils based on the Terzaghi theory, as follows:

$$q_{ult} = c_{av}N_c + qN_q + 0.5\gamma B N_\gamma \qquad (7)$$

where,

$$c_{av} = \frac{Hc_1 + H_2c_2}{H + H_2},$$

$$\phi_{av} = \tan^{-1}\left(\frac{H\tan\phi_1 + H_2\tan\phi_2}{H + H_2}\right),$$

$$H_2 = (2B - H)\left(\frac{c_1 + \tan\phi_1}{c_2 + \tan\phi_2}\right)$$

where, B = footing/pile width, H = thickness of the top layer, H_2 = thickness of the part of the bottom layer that contributes to the bearing capacity, q = overburden pressure, c_1 = cohesion of soil in the top layer, c_2 = cohesion of soil in the bottom layer, ϕ_1 = angle of friction of soil in the top layer, ϕ_2 = angle of friction of soil in the bottom layer, γ_1 = unit weight of soil in the top layer, N_c, N_q and N_γ are bearing capacity factors based on ϕ_{av}.

Azam and Wang (1991) investigated the bearing capacity of an embedded strip footing supported by two-layer c-ϕ soils using an elastoplastic finite-element computer program. Based on the analysis results, they developed a

semiempirical equation for determining the ultimate bearing capacity, as follows:

$$q_0 = q_t + (q_b - q_t)\left[1 - m(H/B)\right]^2 \tag{8}$$

q_0 = end bearing capacity of IESP.
q_t = end bearing capacity in an infinitely thick top-layer soil.
q_b = end bearing capacity on an infinitely thick bottom-layer soil.
$m = 0.17$–0.23 for two layers of clay and 0.30 for a sand-clay layer combination.
H/B = top-layer-thickness-to-footing-width ratio.

Table 1 provides an overview of the different methods and the associated advantages and disadvantages with respect to the estimation of the end bearing capacity of IESP.

3. Constitutive equations for rigid plastic finite element method

The rigid-plastic finite element method (RPFEM) was developed for geotechnical engineering by Tamura et al. (1984, 1987). In this method, the limit load is calculated without any assumption of a potential failure mode. The method is effective in calculating the ultimate bearing capacity of shallow foundations and deep foundations where the soil conditions are varied, such as in multi-layered ground.

In this study, the in-house RPFEM code developed and upgraded by Hoshina et al. (2011) and Du et al. (2016), is used for estimation of the end bearing capacity of a single Incompletely End-Supported Pile. The rigid plastic constitutive equation for the Drucker-Prager yield function was employed first. Then, the non-linear shear strength property against confining pressure, introduced by Du et al. (2016) in RPFEM, was considered. The Drucker-Prager yield function is expressed with Eq. (9) and for considering the non-linear shear strength property against confining pressure, Eq. (10) referred to as the High Order yield function was used. Both yield functions are used in plane strain conditions considering the associated flow rule. Since the plane strain condition is used, the simulated end bearing capacity is that of a continuous wall, however, by employing shape factors, it can be converted to the end bearing capacity of a pile.

$$f(\sigma) = \alpha_{DP} I_1 + \sqrt{J_2} - \kappa = 0 \tag{9}$$

$$f(\sigma) = a I_1 + (J_2)^n - b = 0 \tag{10}$$

where, $I_1 = \mathrm{tr}(\sigma_{ij})$ is the first invariant, $J_2 = \frac{1}{2} s_{ij} s_{ij}$, ν_{DP}, κ, a and b are soil parameters. α_{DP} and κ are expressed for plane strain condition, as follows:

$$\alpha_{DP} = \frac{\tan\phi}{\sqrt{9 + 12\tan^2\phi}}, \quad \kappa = \frac{3c}{\sqrt{9 + 12\tan^2\phi}} \tag{11}$$

where c is cohesion, ϕ is shear resistance angle.

The parameters n, a and b in the High Order yield function Eq. (10) are coefficients representing the non-linear shear strength property against confining pressure for the soil; n is standing for the strength non-linearity; a and b are relating to the shear resistance angle ϕ and the cohesion c, respectively. As a remark, when n in the High Order yield function is 0.5 the two Equations, Eq. (9) and Eq. (10) are the same. When n is higher than 0.5, the plot of $\sqrt{J_2}$ against I_1 gives a linear line with Eq. (9), but a curved line with Eq. (10) (see Fig. 3).

For the Drucker-Prager yield function, the volumetric strain rate for the Rigid Plastic constitutive equation is expressed, as follows:

$$\dot{\varepsilon}_v = \mathrm{tr}(\dot{\varepsilon}) = \mathrm{tr}\left(\lambda \frac{\partial f(\sigma)}{\partial \sigma}\right) = \mathrm{tr}\left(\lambda\left(\alpha I + \frac{s}{2\sqrt{J_2}}\right)\right)$$
$$= \frac{3\alpha}{\sqrt{3\alpha^2 + \frac{1}{2}}} \dot{e} \tag{12}$$

where λ is the plastic multiplier and $\dot{e}$ is the norm of the strain rate. I and s express the unit and the deviator stress tensors, respectively. The strain rate $\dot{\varepsilon}$, which is a purely plastic component, should satisfy the volumetric constraint condition which is derived by Eq. (13), as follows:

$$h(\dot{\varepsilon}) = \dot{\varepsilon}_v - \frac{3\alpha}{\sqrt{3\alpha^2 + \frac{1}{2}}} \dot{e} = \dot{\varepsilon}_v - \eta \dot{e} = 0 \tag{13}$$

Any strain rate which is compatible with the Drucker–Prager yield criterion must satisfy the kinematic constraint conditions of Eq. (13). η is a coefficient determined by Eq. (13) which is one of the dilation characteristics. The rigid plastic constitutive equation is expressed by the Lagrangian method after Tamura et al. (1987), as follows:

$$\sigma = \frac{\kappa}{\sqrt{3\alpha^2 + \frac{1}{2}}} \frac{\dot{\varepsilon}}{\dot{e}} + \beta\left(I - \eta \frac{\dot{\varepsilon}}{\dot{e}}\right) \tag{14}$$

The first term expresses the stress component, uniquely determined for the yield function. The second term expresses the indeterminate stress component along with the yield function. The indeterminate stress parameter β remains unknown until the boundary value problem with Eq. (13) is solved. In this study, a penalty method is used to make the computation faster and more stable following Hoshina et al. (2011), as follows:

$$\sigma = \frac{\kappa}{\sqrt{3\alpha^2 + \frac{1}{2}}} \frac{\dot{\varepsilon}}{\dot{e}} + P(\dot{\varepsilon}_v - \eta \dot{e})\left(I - \eta \frac{\dot{\varepsilon}}{\dot{e}}\right) \tag{15}$$

where P is a penalty constant.

For the High Order yield function, based on the associated flow rule, the strain rate is obtained as follows:

$$\dot{\varepsilon} = \lambda \frac{\partial f(\sigma)}{\partial \sigma} = \lambda \frac{\partial}{\partial \sigma}\left(a I_1 + (J_2)^n - b\right)$$
$$= \lambda\left(a I + n(J_2)^{n-1} s\right) \tag{16}$$

Table 1
Application conditions and limitations of the existing methods.

Formula	Disadvantages with respect to the estimation of the end bearing capacity of IESP	Advantages with respect to the estimation of the end bearing capacity of IESP
Eq. (2): Terzaghi (1943), Vesić (1967) and Meyerhof (1976)	• Cannot directly estimate the end bearing capacity of IESP alone.	• Can be used to calculate q_{base} and q_{nobase} of Hyodo et al. (2020)Can be used to calculate q_b and q_t of Azam and Wang (1991)N_c and N_q of Eq. (2) can be used in Satyanarayana and Garg (1980)
Eq. (5): Hyodo et al. (2020)	• Applicable for sand only.Does not consider the strength ratio of the two soil layers.	• Gives a reasonable end bearing capacity of IESP in sand.
Eq. (6): Satyanarayana and Garg (1980)	• Using average values of strength parameters (not realistic).	• Can be used for any type of soil and gives reasonable results.
Eq. (7): Azam and Wang (1991)	• Does not consider the strength ratio of the two soil layers.	• Can be used for any type of soil and gives reasonable results.

In the above equation, λ is the plastic multiplier. The volumetric strain rate is expressed as:

$$\dot{\varepsilon}_v = \mathrm{tr}(\dot{\varepsilon}) = \mathrm{tr}\left(\lambda\left(a\boldsymbol{I} + n(J_2)^{n-1}\boldsymbol{s}\right)\right) = 3a\lambda$$

$$= \frac{3a}{\sqrt{3a^2 + 2n^2(b - aI_1)^{2-1/n}}}\dot{e} \qquad (17)$$

First, the stress invariant I_1 is identified from Eq. (17) using the following equation:

$$\boldsymbol{I}_1 = \frac{b}{a} - \frac{1}{a}\left\{\frac{1}{2n^2}\left[\left(3a\frac{\dot{e}}{\dot{\varepsilon}_v}\right)^2 - 3a^2\right]\right\}^{\frac{n}{2n-1}} \qquad (18)$$

The non-linear rigid plastic constitutive equation for the High Order yield function is finally obtained as follows:

$$\sigma = \frac{3a}{n}\left\{\frac{1}{2n^2}\left[\left(3a\frac{\dot{e}}{\dot{\varepsilon}_v}\right)^2 - 3a^2\right]\right\}^{\frac{1-n}{2n-1}}\frac{\dot{\varepsilon}}{\dot{\varepsilon}_v}$$

$$+ \left(\frac{b}{3a} - \frac{1}{3a}\left[\frac{1}{2n^2}\left(3a\frac{\dot{e}}{\dot{\varepsilon}_v}\right)^2 - 3a^2\right]^{\frac{n}{2n-1}}\right.$$

$$\left. - \frac{a}{n}\left[\frac{1}{2n^2}\left(3a\frac{\dot{e}}{\dot{\varepsilon}_v}\right)^2 - 3a^2\right]^{\frac{1-n}{2n-1}}\right)\boldsymbol{I} \qquad (19)$$

In this equation, the stress is uniquely determined for the plastic strain rate and is different from Eq. (15) for the Drucker-Prager yield function.

The advantage of the rigid plastic constitutive equation is that it requires only a few soil parameters, such as unit weight, cohesion and shear resistance angle. In the simulation, the pile is modeled by the rigid plastic constitutive equation as rigid material to focus on the plastic behavior of the soils around the pile subjected to vertical loading. Therefore, the elastic modulus and Poisson's ratio are not necessary for this simulation method, and it is not specific to a certain type of pile. In addition, since the high order yield function considers the reduction of the shear resistance angle due to high confining pressure, it avoids over-
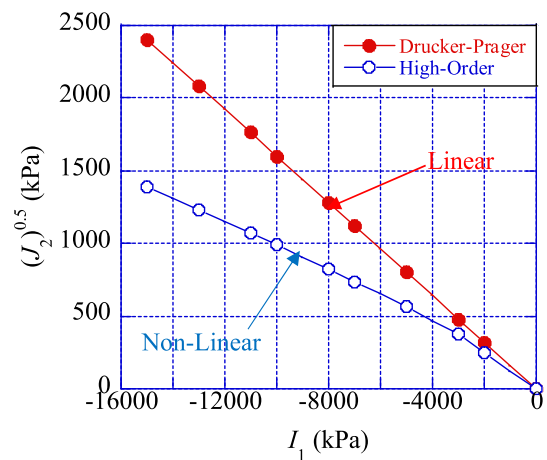

Fig. 3. Difference between the yield function of Drucker-Prager the and High-Order model.

estimating the volumetric strain in ϕ and c-ϕ soils and therefore provides more reasonable end-bearing capacity values for piles in those soils.

4. Finite element mesh and boundary conditions

An illustration of the finite element mesh and the boundary conditions used is shown in Fig. 4. First, a hollow model and a joint elements model were used to check the interaction between the end capacity and skin friction. In both models, a soft soil layer underlain by a hard soil layer was modeled. For the hollow model, a hollow was used in lieu and place of a pile. For the joint elements model, joint elements were used between the pile and the surrounding. To estimate both the end capacity and friction simultaneously, the characteristics of the joint elements were set at the same as those of the surrounding ground. To estimate the end capacity separately, the characteristics of the joints were chosen to allow a smooth condition. This is the same as the method used by Hyodo et al. (2020). A mesh of approximately 7000 rectangular elements was used to represent each model. The boundary conditions were set large enough to simulate an infinite soil mass.

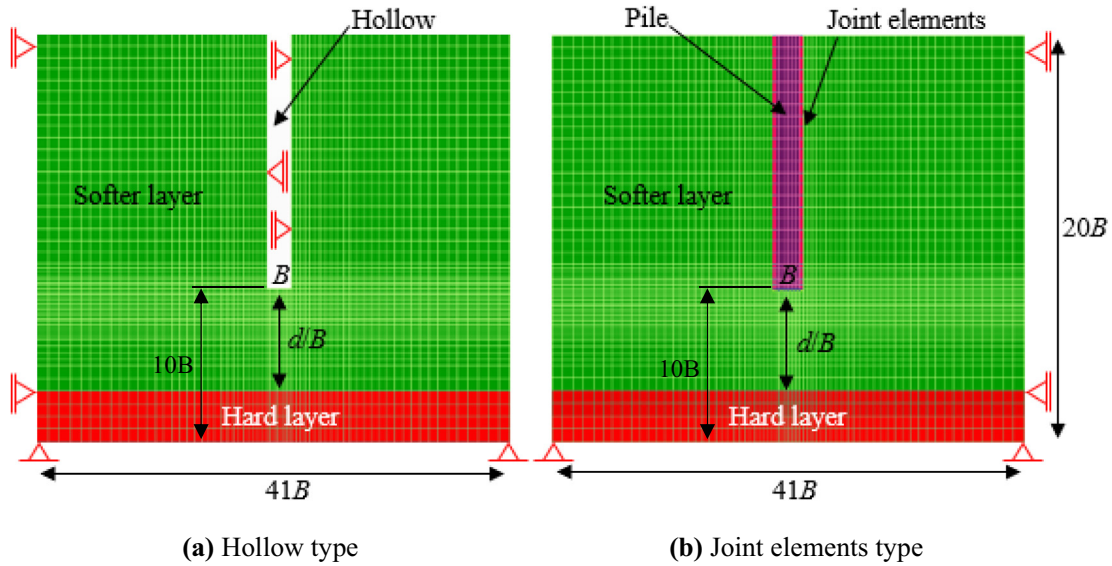**(a)** Hollow type   **(b)** Joint elements type

Fig. 4. Mesh and boundary conditions used for simulation by (a) using hollow and (b) joint elements.

The density of the mesh elements was refined near the pile to capture the higher expected strain. The left and right sides of the domain were pinned, and the bottom boundary of the domain was fixed. An increasing load in a downward direction was applied. The normalized distance between the hollow bottom/pile tip and the hard soil layer (d/B) was varied.

5. Validation of the simulation methode

The simulation method is validated against the experimental results reported by Pholkainuwatra et al. (2022) from their study of the pile set-up of driven piles in Bangkok clay (c soil). The soil conditions in their study are depicted in Fig. 5. These soil conditions are used to simulate the end bearing capacities with RPFEM using the

Drucker-Prager yield function. Fig. 5(c) shows the comparison of end bearing capacities on the 32nd day after pile installation obtained by Pholkainuwatra et al. (2022) and the simulation results. Good agreement was found between the simulation results of this study and the findings of Pholkainuwatra et al. (2022), as can be observed in Fig. 5 (c). This comparison suggests that the simulation method used in this study is reliable enough.

6. Analysis based on the drucker prager yield function

6.1. Analysis parameters for estimating the bearing capacity of IESP

The simulation was done for a cohesive soil (c soil), cohesionless soil (ϕ soil) and an intermediate soil (c-ϕ soil).
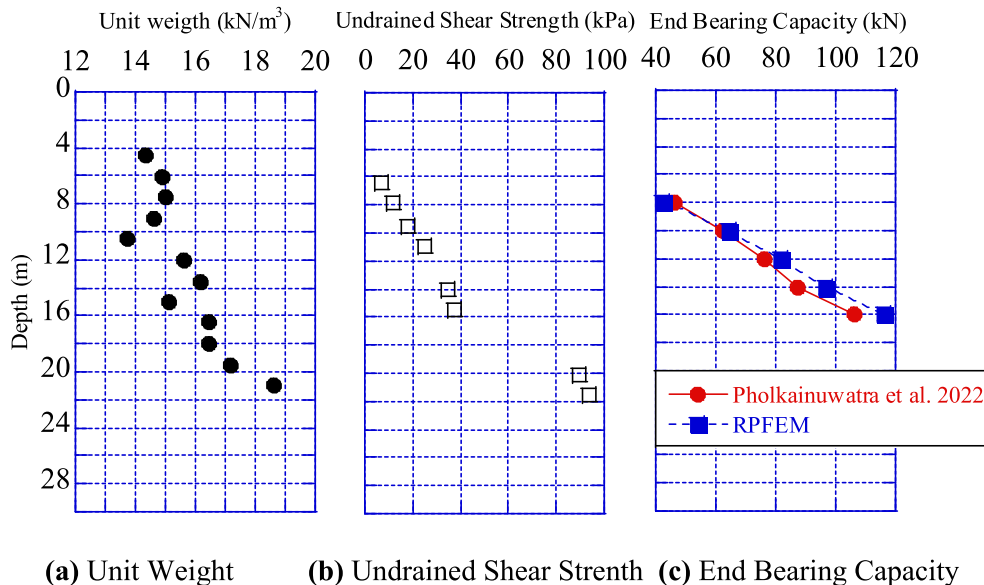

(a) Unit Weight   **(b)** Undrained Shear Strenth   **(c)** End Bearing Capacity

Fig. 5. Validation of the simulation method against Pholkainuwatra et al. (2022).

Table 2
Soil characteristics.

Soil type	Layers	ϕ (deg.)	c (kPa)	γ (kN/m^3)
c soil	Soft layer	0	25	14
	Hard layer	0	75	17
ϕ soil	Soft layer	30	0	17.5
	Hard layer	40	0	20
c-ϕ soil	Soft layer	20	45	17
	Hard layer	35	10	19

Table 2 shows the soil parameters for each type of soil used in these simulation cases. These specific values are used only to illustrate the behavior of the bearing capacity. Later in this study, the bearing capacity ratio, which is a non-dimensional parameter, will be used by varying the soil parameters. The pile in this simulation has the following properties: cohesion $c = 50,000$ kPa, shear resistance angle $\phi = 0$ degrees and unit weight $\gamma = 25$ kN/m^3 to make the pile a rigid non-deformable body based on Hoshina et al. (2011) and Du et al. (2016). The pile length, as well as the embedment length, are set constant (with a slenderness of 10B). The unit weight of the overburden layer is also considered in the simulation. Since water is not considered, the effective stress is equal to the total stress. In the case of ϕ soil and c-ϕ soil, the peak shear strength indicates the problem is under a long-term condition, whereas c soil is under the undrained condition, which is like a short-term condition. The main parameter was the distance (d/B), the distance between the pile tip and the bottom layer (d) was normalized by the pile width (B). The influence of this parameter on the total bearing capacity, the end bearing capacity and the skin friction was investigated. Note that the influence of d/B illustrates the influence of the bottom layer.

6.2. Bearing capacity of IESP

The variation of the bearing capacity of IESP as a function of the normalized distance d/B is shown in Fig. 6. The negative values of d/B indicate that the pile has penetrated the bottom hard soil layer. Note that these negative values of d/B are used just to confirm the effect of the penetration into the bottom layer with higher strength. The main concern in this study is to determine where the deficiency of bearing capacity happens, when $d/B > 0$. The two simulation methods (Hollow and Joint) coincide for all three soil types.

For the three soil types, the skin friction contributes considerably to the total bearing capacity. The total bearing capacity and the end bearing capacity decrease with the increasing value of d/B, however, the influence of d/B on the skin friction is very small and therefore negligible. These observations mean that the bottom layer greatly influences the end bearing capacity but does not much affect the skin friction. Since the main objective of this study is to investigate the influence of the bottom layer, the end bearing capacity becomes the main concern.

The decrease of the end bearing capacity expresses the degradation of the end bearing capacity when the pile moves away from the bottom layer. The end bearing capacity attains a minimum steady value, equal to that of the top layer, over approximately three times the pile diameter (critical distance $d/B^* = 3$). This value on critical distance is in good agreement with the result of Houlsby et al. (1994) who studied the end bearing capacity of pile in homogeneous uncemented sand within which a horizontal cemented carbonate sands layer was inserted as a bearing layer (see Fig. 7).

6.3. The end bearing capacity ratio (analyses parameters)

An end bearing capacity ratio r is defined as the ratio of the end bearing capacity of the case $d/B = 0$ (pile tip on the bottom layer), namely q_H, to the end bearing capacity of the pile when the bottom layer has no influence, namely q_s (Eq. (20)). q_s also represents the end bearing capacity of a uniform ground made of the top softer soil layer. By changing the soil parameters of the bottom soil layer, the following ratios r are obtained: for c soil $r = 1.68$–4.20; for ϕ soil $r = 1.55$ to 3.8 and for c-ϕ soil $r = 1.45$ to 6.35. The soil parameters used widely cover the values expected in practical engineering and are presented in Table 3. The effect of changing the ratio r on the end bearing capacity was then investigated usin g the following:

$$r = \frac{q_H}{q_s} \qquad (20)$$

6.4. Influence of the end bearing capacity ratio

The behavior of the end bearing capacities for different values of the ratio r (Eq. (20)) were studied and the results were normalized using Eq. (21). In Eq. (21), $q_{(d/B^*)}$ is the end bearing capacity at the critical distance (d/B^*) and is also equal to the end bearing capacity of the pile when the bottom layer has no influence (q_s) (Fig. 6). q_0 is the end bearing capacity of the case of $d/B = 0$, which is the end bearing capacity when the pile tip is on the surface of the bottom soil layer (q_H) and q_x is the end bearing capacity corresponding to a given distance, $d/B = \boldsymbol{x}$.

$$\xi_x = \frac{q_x - q_{(d/B^*)}}{q_0 - q_{(d/B^*)}} = \frac{q_x - q_s}{q_H - q_s} \qquad (21)$$

Fig. 8 shows the influence of the ratio r on the end bearing capacity for the three soils. The end bearing capacity increases with the increase of the ratio r. However, the influence of r is different depending on the soil type. A non-influence of r is observed when $d/B > 0.5$ for c soil, $d/B > 1.5$ for ϕ soil and $d/B > 1.25$ for c-ϕ soil. From these results, it is found that the degradation of the end bearing capacity is influenced by the ratio r. For small values of r, the degradation is smooth, however, for high values of r, the degradation is sudden. The sudden degradation in the cases of high values of r is due to the sudden change of

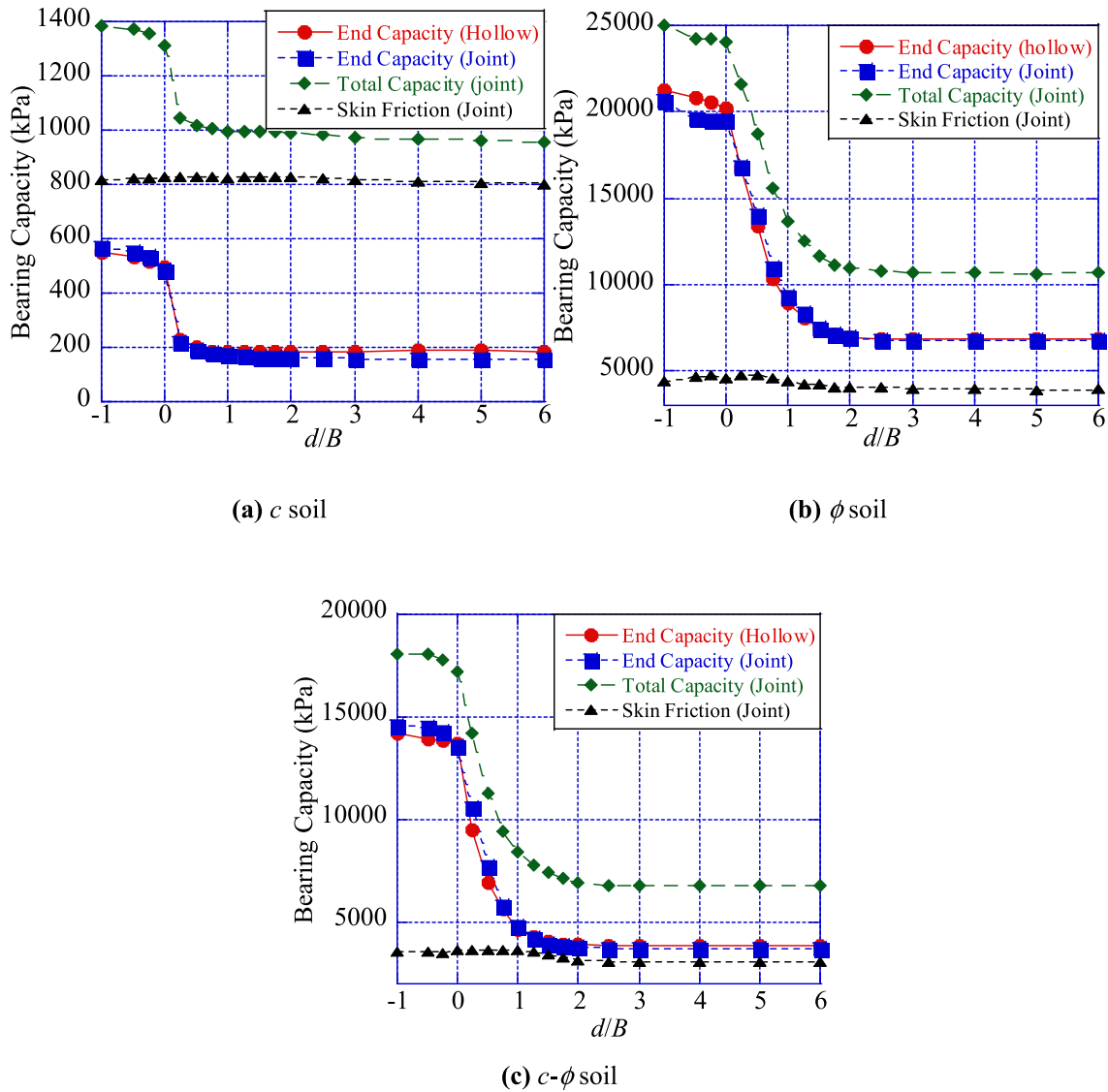**(a)** c soil

(b) ϕ soil

(c) c-ϕ soil

Fig. 6. Influence of the distance between the pile tip and the surface of the hard layer on the end bearing capacity of IESP.

the end bearing capacity from very high ($d/B \leq 0$) to relatively very small (when $d/B > 0$). The normalized end bearing capacities are depicted in Fig. 9 for the three soils. The normalized end bearing capacities represent the degradation factors of the end bearing capacity when the pile goes away from the hard bottom layer. The degradation factor ξ_x inversely increases with the ratio r, a non-influence is observed around $d/B = 3$. The degradation factor ξ_x is also influenced by the soil type as the slopes of ξ_x testify in Fig. 9. The slopes of c soil are the steepest, followed by those of c-ϕ soil and the slopes of ϕ soil are not as steep.

6.5. Failure patterns

Several of the proposed failure mechanisms proposed are shown in Fig. 10.

The strain rate distribution styles based on the Drucker-Prager yield function using the joint elements numerical model are shown in Fig. 11, Fig. 12 and Fig. 13 for the

three types of soils in Table 2. The norm of the strain rate is represented by contour lines in the range of $\dot{e}_{max} \sim \dot{e}_{min}$ (=0). The boundary conditions are sufficient since the strain rate did not reach the limits of the domain. The failure pattern is different for each type of soil. This difference might explain the difference in the value of d/B from which the ratio r has no influence for each soil type in Fig. 8 and the difference in the slopes of ξ_x in Fig. 9. When the distance $d/B < d/B* = 3$, the yield zones at the collapse stage extend into the bottom layer, and the higher strength of the bottom layer therefore contributes to a greater end bearing capacity. However, for $d/B > d/B*$, the yielding is confined into the top layer, as a result, the lower strength of the top layer reduces the end bearing capacity.

The shear bands obtained with c soil are similar to case (a) and case (b) in Fig. 10. However, in the case of ϕ soil and c-ϕ soil, all the shear bands are not ideally like those in Fig. 10. The shear bands are observed to be widespread in the case of ϕ soil and c-ϕ soil. This phenomenon can be
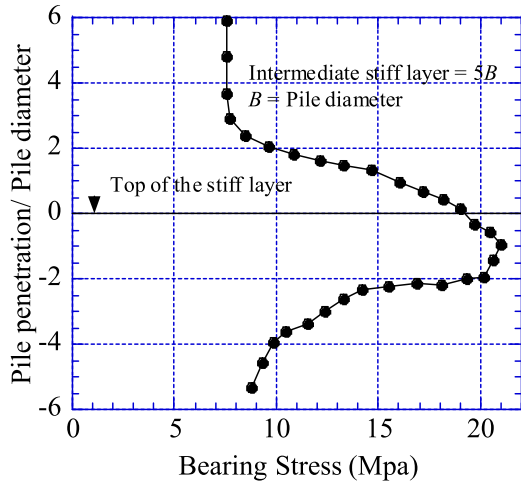
Fig. 7. Bearing capacity against depth obtained by Houlsby et al. (1994) for an intermediate stiff soil layer placed within a softer soil.

Table 3
Soil parameters of the bottom hard layer and equivalent end bearing capacity ratios.

(a) For c soils, with c = 10 kPa, ϕ = 0 degrees and γ = 13.5 kN/m^3 as parameters of the top layer

End bearing capacity ratio (r)	ϕ (deg.)	c (kPa)	γ(kN/m^3)
1.68	0	40	15
2.13	0	50	16
3.19	0	75	17
3.79	0	90	17.5
4.20	0	100	18

(b) For ϕ soils, with, c = 1 kPa, ϕ = 30 degrees and γ = 17.5 kN/m^3 as parameters of the top layer

End bearing capacity ratio (r)	ϕ (deg.)	c (kPa)	γ (kN/m^3)
1.55	34	1	18
1.95	36	1	18.5
2.42	38	1	19
3.10	40	1	20
3.80	42	1	21

(c) For c-ϕ soils, with, c = 45 kPa, ϕ = 20 degrees and γ = 17 kN/m^3 as parameters of the top layer

End bearing capacity ratio (r)	ϕ (deg.)	c (kPa)	γ (kN/m^3)
1.45	25	30	17
2.25	30	20	17.5
2.82	32	15	18
3.75	35	10	19
6.35	40	5	20

attributed to the fact that the influence of the confining pressure on the shear resistance angle is not considered in the Drucker-Prager yield function, leading to the overestimation of the volumetric strain. On the other hand, since the shear resistance angle of the c soil is zero (0), this does not affect the c soil. Hence, the shear bands of c soil are similar to those in case (a) and case (b), shown in Fig. 10.

The shear bands observed in ϕ soil and c -ϕ soil suggest that the Drucker-Prager yield function overestimates the end bearing capacity for ϕ soils and c -ϕ soils. Since the High order yield function considers the influence of the

confining pressure on the shear resistance angle, it may provide more reasonable end-bearing capacity values of IESP. That is, an analysis method using the High order yield function is required.

7. Analysis based on the high order yield function

7.1. Influence of the confining pressure on the shear resistance angle

Du et al. (2016) improved RPFEM using the High Order yield function to introduce the non-linear shear strength property against confining pressure in order to consider the influence of particle breakage. The High Order yield function, therefore, remedies the problems related to high confining pressure, particle breakage, and the overestimation of end bearing capacity of piles in soils with a shear resistance angle.

The shear resistance angle of soil decreases with increasing confining pressure, as shown in Figs. 14 and 15. Hettler and Gudehus (1988) have proposed Eq. (22) as a formula to express the decrease in the shear resistance angle ϕ with an initial angle ϕ*:

$$\phi = \arcsin \frac{sin\phi^*}{\left(\frac{\sigma_2}{\sigma_{20}}\right)^\zeta + sin\phi^*\left[1 - \left(\frac{\sigma_2}{\sigma_{20}}\right)^\zeta\right]} \tag{22}$$

where σ_2 is the lateral stress, ζ is estimated from triaxial tests, ϕ* is the shear resistance angle for the reference lateral stress. ζ is close to 0.1 and remains unchanged for various sands and densities.

Eq. (22) is used in this study to consider the decrease of the shear resistance angle due to the high confining pressure. Instead of σ_{20} and σ_2, I_{10} and I_1 were considered to represent the confining pressure, as shown in Fig. 15. This equation cannot be directly applied to the boundary value problems because it was proposed based on the triaxial tests. However, the reduction in the shear resistance angle can be modeled for any given reference confining stress I_1. Based on Eq. (22) the obtained decrease of the shear resistance angle was then taken as a reference to determine the coefficients a, b and n in the high order yield function (Eq. (10)).

Figs. 16 and 17 show the estimated results of the coefficients for the following soils: the top layer and the bottom layer of the ϕ soil and c-ϕ soil. It can be confirmed that the reference curve based on Helter-Gudehous (1988) can be reproduced accurately. The coefficients for the soils used in the simulation are listed in Table 4.

7.2. Comparison of end bearing capacities of IESP from the two yield functions

By using the nonlinear shear strength parameters (n, a and b) shown in Table 4, the end bearing capacity of IESP was simulated with the high order yield function.

(a) c soil

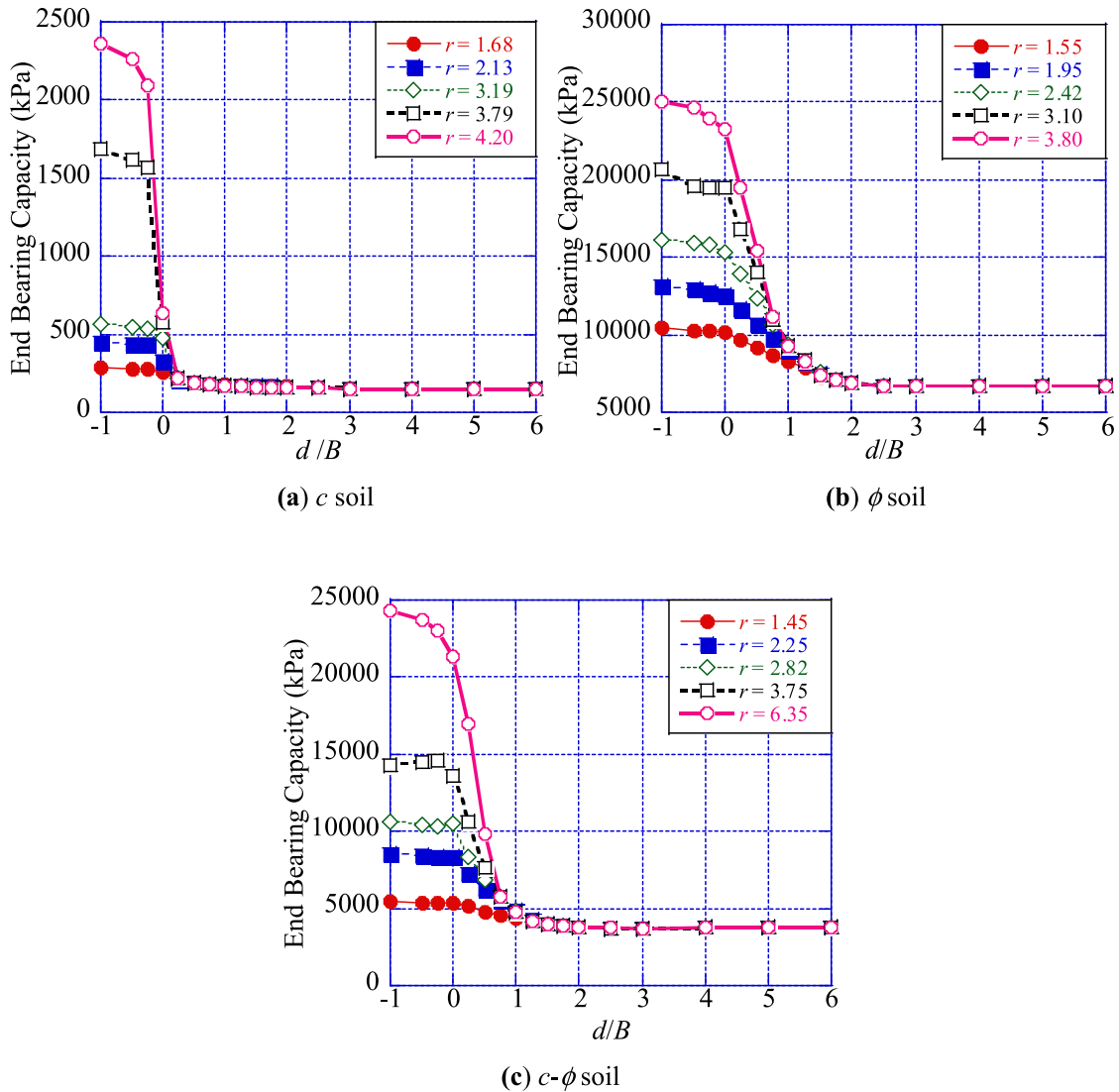**(b)** ϕ soil

(c) c-ϕ soil

Fig. 8. Influence of the ratio r on the end bearing capacity of IESP.

The variation of the end bearing capacity of IESP as a function of the distance d/B is shown in Fig. 18. Independently, with the yield function used and the type of soil, the end bearing capacity decreases with the increase of d/B. It attains a minimum steady value at a critical distance $d/B^* = 3$.

The results from the Drucker-Prager yield function are greater than those from the High Order yield function. The difference between the results from the two yield functions is greater when the pile approaches the hard layer (range of $d/B < 3$). This can be explained by the influence of the hard layer in that range of d/B, the non-linear shear strength property against confining pressure is explicitly observed.

Fig. 19 compares the degradation factors ξ_x of Drucker-Prager and High-Order yield functions. For all the cases, roughly one curve is obtained for each soil type, independently of the yield functions. This means that the values

of the degradation factor ξ_x do not depend on the yield function used.

7.3. Failure patterns

The strain rate distribution style obtained with the High Order yield function is shown in Fig. 20 and Fig. 21 for ϕ soil and c-ϕ soil, respectively. The norm of the strain rate is presented by the contour lines in the range of $\dot{e}_{max} \sim \dot{e}_{min}$ ($=0$). As in the case of Drucker-Prager yield (Fig. 12 and Fig. 13), for both soil types, when the distance $d/B < 3$, the yield zones at the collapse stage extend into the bottom layer. However, when $d/B \geq 3$, the yielding is confined to the top layer, and the shear bands obtained with the High Order yield function are all similar to the case (a) and (c) in Fig. 10. The shear bands obtained with the High Order yield function are ideal and are more reliable than those

(a) c soil
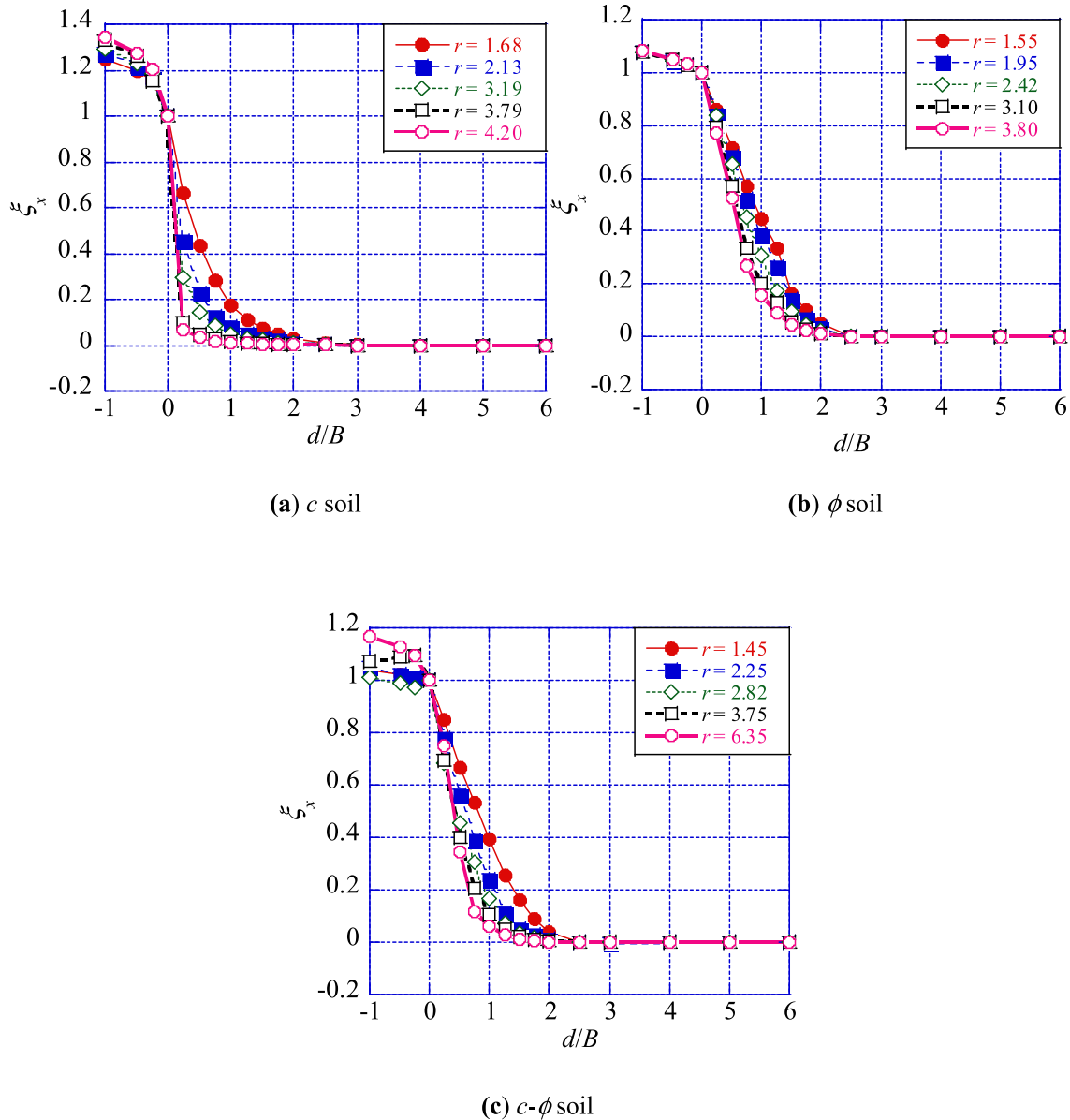
(b) ϕ soil

(c) c-ϕ soil

Fig. 9. Normalization of the end bearing capacities with different end bearing capacity ratios.

obtained with the Drucker-Prager yield function (Figs. 12 and 13).

7.4. Justification of the differences between the results obtained with the two simulations methods

Figs. 22 and 23 show the stress state (the relationship between the I_1 and $\sqrt{J_2}$) of all elements obtained by RPFEM for ϕ soil and c-ϕ soil, respectively.

For each soil layer of both soil types, the simulation with Drucker-Prager (D.P.) gives higher values of I_1 and $\sqrt{J_2}$. The lower values of I_1 and $\sqrt{J_2}$ of the simulations with H.O. justify the localization of the generation of the strain rate due to the reduction of the shear resistance angle and the dilation, angle as shown in the failure patterns

(Fig. 20 and Fig. 21). This results in the lower end bearing capacity in the simulations with H.O.

According to the simulation results, the difference between D.P. and H.O. is more significant in ϕ soil than in c-ϕ soil. This suggests that the influence of confining pressure on the shear resistance angle is more significant in ϕ soil, less significant in c-ϕ soil and absent in c soil (since $\phi = 0$ deg. in c soil).

Comparing the simulation results of the case $d/B = 1$ and the case $d/B = 3$, as the pile nears the bottom layer, a higher stress is induced by the load in the ground at the failure stage (I_1). The stress at the failure stage is higher in the top layer than in the bottom layer, and this difference is more significant for greater values of d/B. This is because the stress caused by the total load is higher near the pile tip. It may be noticed that at $d/B = 3$, the stress in the bottom
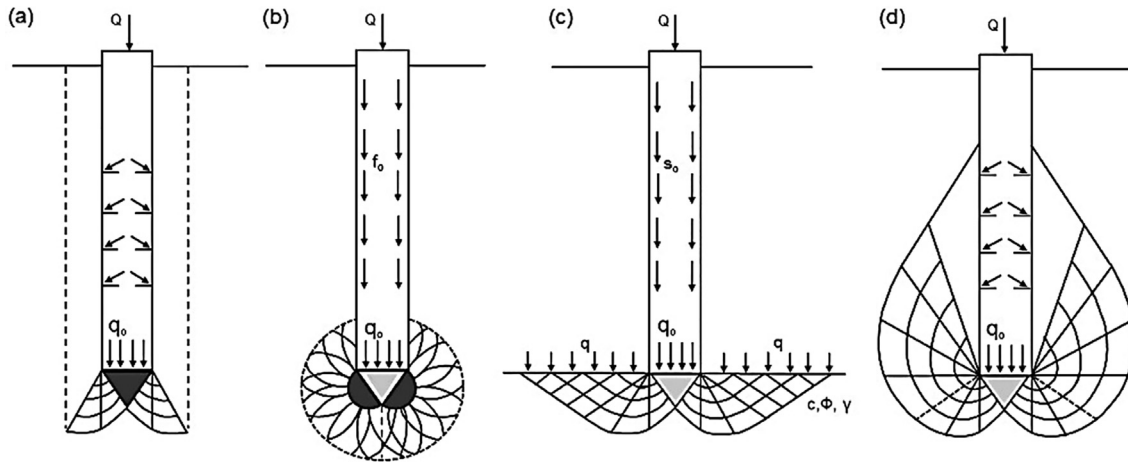
Fig. 10. Different failure patterns around the pile tip assumed by different researchers (Veiskarami et al (2011)): (a) Berezantzev and Yaroshenko (1962), Vesic (1963); (b) Bishop et al. (1945), Skempton et al. (1953); (c) Prandtl (1920), Reissner (1924), Caquot (1934), Buisman (1935), Terzaghi (1943); (d) De Beer (1945), Jáky (1948), Meyerhof (1951).
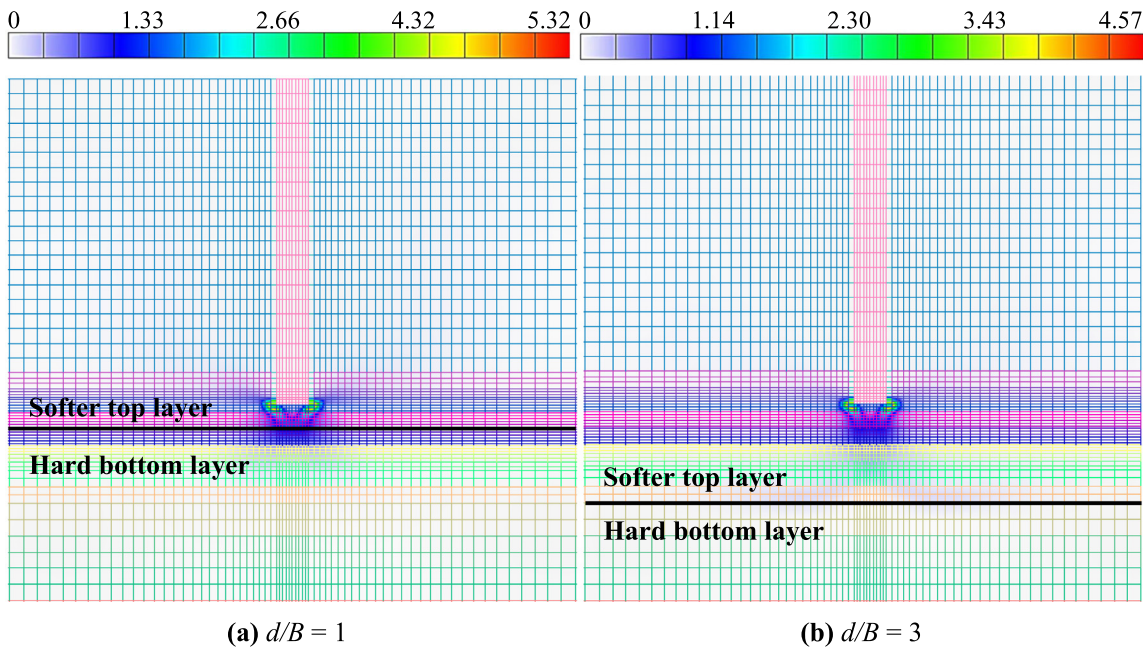

(a) $d/B = 1$ **(b)** $d/B = 3$

Fig. 11. Strain rate distribution from c soil using Drucker Prager.

layer is almost insignificant. These facts explain the decrease of the end bearing capacity with the increasing d/B and the non-influence of the bottom layer when $d/B \geq 3$.

8. Formula for estimation of the end bearing capacity of IESP

This formulation in Eqs. (23) and (24) are proposed as a formula to estimate the end bearing capacity of IESP.

$$q_x = \xi_x q_H + (1 - \xi_x)q_s = \xi_x(q_H - q_s) + q_s \qquad (23)$$

$$\xi_x = \frac{q_x - q_s}{q_H - q_s} \qquad (24)$$

where q_x is the end bearing capacity when $d/B = x$, q_H is the end bearing capacity when $d/B = 0$, q_s is the end bearing capacity of the pile when the bottom layer has no influence and ξ_x is the degradation factor.

q_H and q_s can easily be obtained by an analytical or numerical method. However, the values of ξ_x need to be estimated independently of q_x.

For the formula of estimating ξ_x, Eq. (25) is proposed based on the above simulation results. Where d/B is the normalized distance between the pile tip and the surface of the bottom layer and m is a coefficient that depends on soil type and the end bearing capacity ratio r.

For the different values of r of each soil type, Eq. (24) was used to obtain ξ_x: this was plotted as a function of

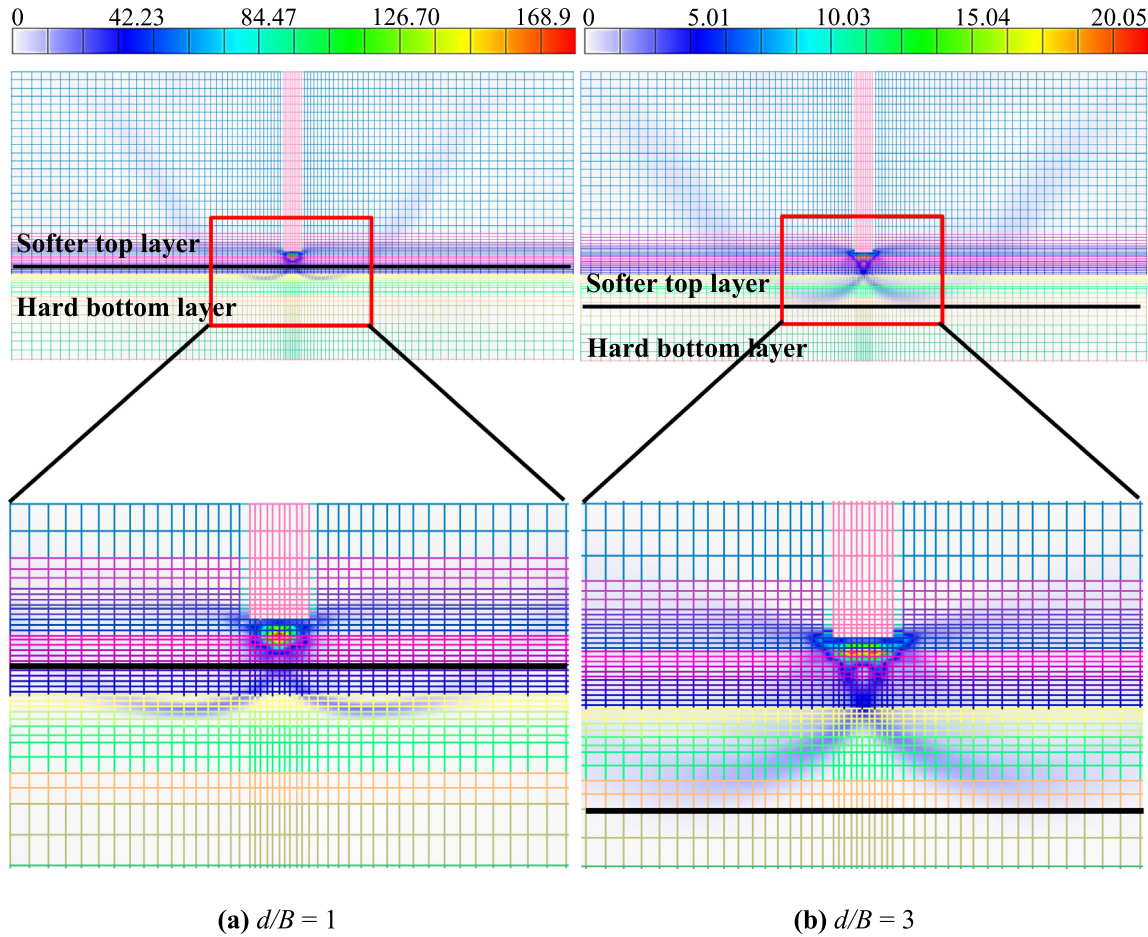**(a)** $d/B = 1$ **(b)** $d/B = 3$

Fig. 12. Strain rate distribution from ϕ soil using Drucker Prager.

d/B. The values of m in Eq. (25) are then obtained by fitting the ξ_x of Eq. (25) to those of Eq. (24). Those values of m are plotted and are used as references to propose Eq. (26), Eq. (27) and Eq. (28) for calculating the value of the coefficient m, for c soil, ϕ soil and c-ϕ soil, respectively.

$$\xi_x = \frac{1}{1 + m \cdot (d/B)} \tag{25}$$

$$m_c = 8.3984r - 10.528 \tag{26}$$

$$m_\phi = 5.66 \log(r) + 0.31644 \tag{27}$$

$$m_{c-\phi} = 6.0712 \log(r) + 0.68599 \tag{28}$$

The proposed formula in Eq. (23) is like the formulas of Hyodo et al. (2020) [Eq. (6)] and Azam and Wang (1991) [Eq. (8)]. Table 5 shows the equivalence of the three formulas. In Hyodo et al. (2020) the degradation factor is independent of the end bearing capacity ratio r and applicable to sandy soil only. However, as shown in Fig. 9, the degradation factor is influenced by the ratio r and soil type. This makes the weak point of Hyodo et al. (2020). In Azam and Wang (1991) the coefficient m of the degradation factor changes according to the soil type. The results in this study are in good agreement with those results and makes the strong point of Azam and Wang

(1991). However, m is independent of the bearing capacity ratio r which makes the weak point of Azam and Wang (1991). Therefore, it is thought that the formula proposed in this study have more advantage and applicability than the previous research.

9. Validation of the proposed formula

9.1. Comparison with analytical methods

The results from the proposed formula are compared with those from the methods used by Satyanarayana and Garg (1980) and Azam and Wang (1991). The method of Meyerhof (1976) is used to calculate of q_b and q_t in the Azam and Wang (1991) method and the Meyerhof (1976) bearing capacity factors N_c and N_q are used in Satyanarayana and Garg (1980) method. The soils in Table 2 were used for the comparison.

A bored cast-in-situ pile was considered (without debris at the pile tip). At $d/B = 0$, the bearing layer is the bottom layer, in that case, the actual thickness of the bearing stratum $D_b = 0$.

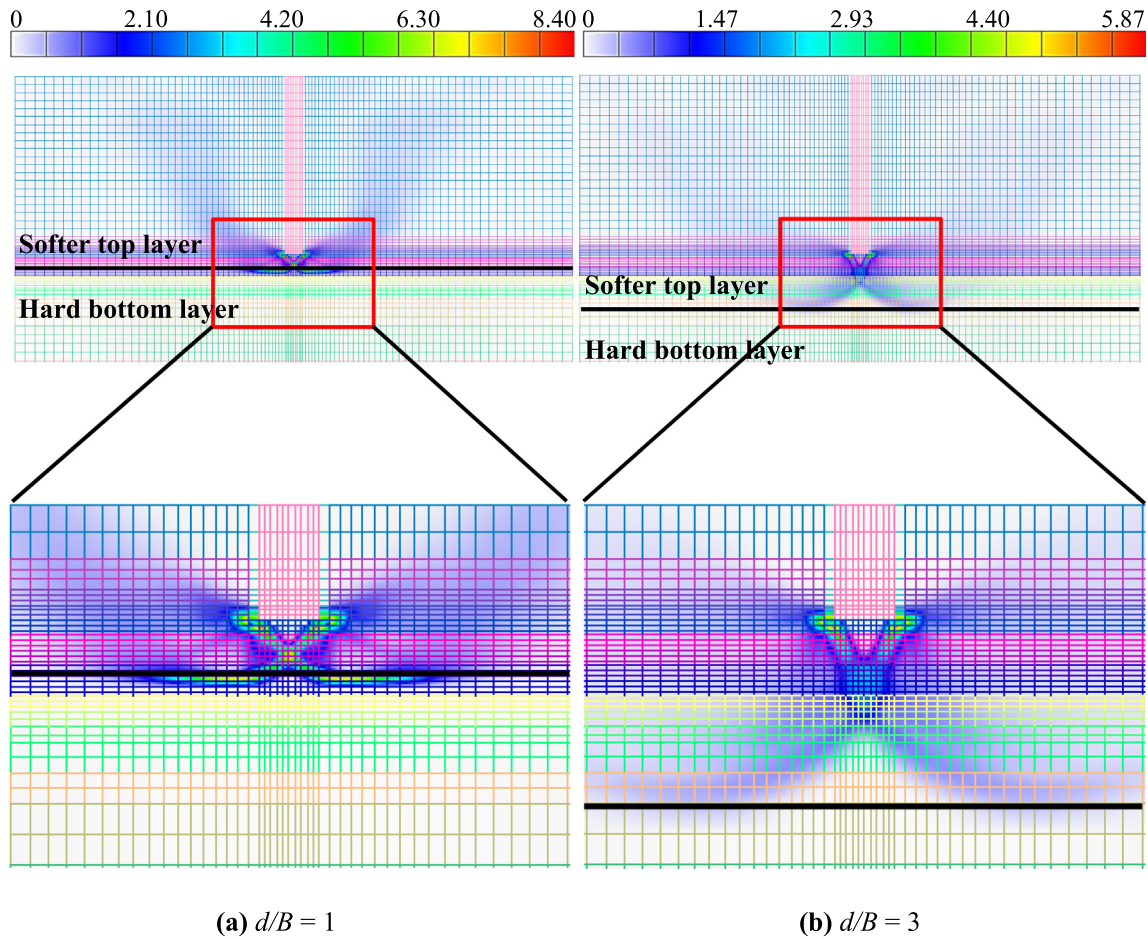The comparison is shown in Fig. 24. When q_s and q_H in the proposed equation are obtained from the RPFEM,

(a) $d/B = 1$ **(b)** $d/B = 3$

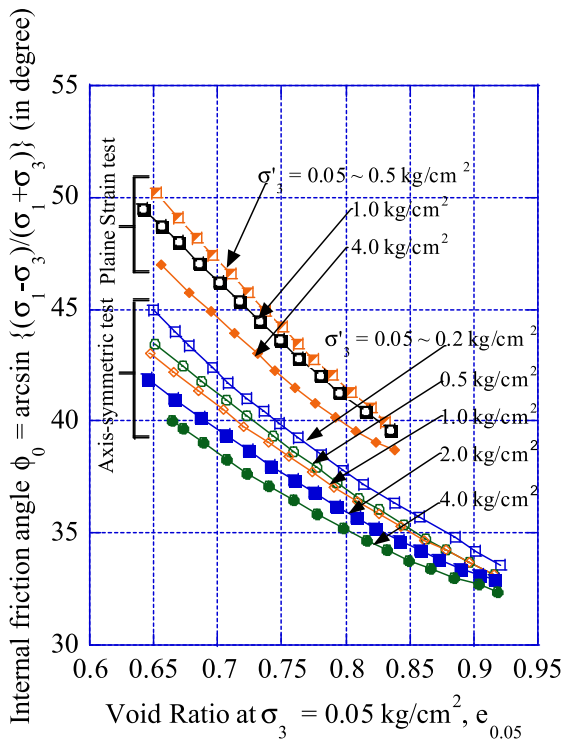Fig. 13. Strain rate distribution from c-ϕ soil using Drucker Prager.

Fig. 14. Effect of the confining pressure on the shear strength through the experiments on Toyoura sand (Tatsuoka et al., 1986).
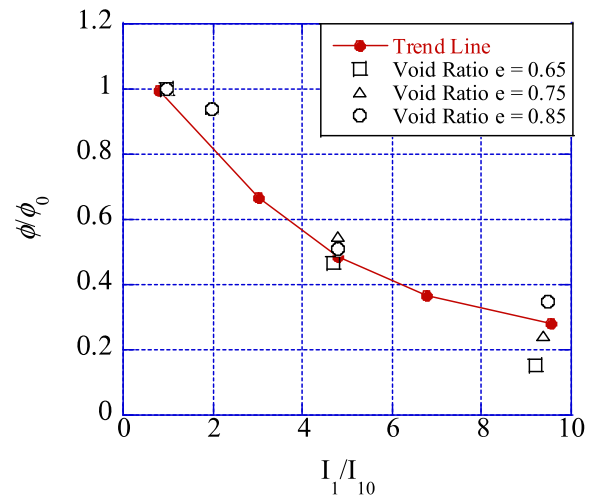

Fig. 15. Relationship between ϕ/ϕ_0 and I_1/I_{10} (Du et al. (2016)).

there is good agreement between the simulation method and the proposed equation.

For c soil, as shown in Fig. 24(a), good agreement is obtained between the Satyanarayana and Garg (1980) method, the proposed equation and RPFEM using D.P.
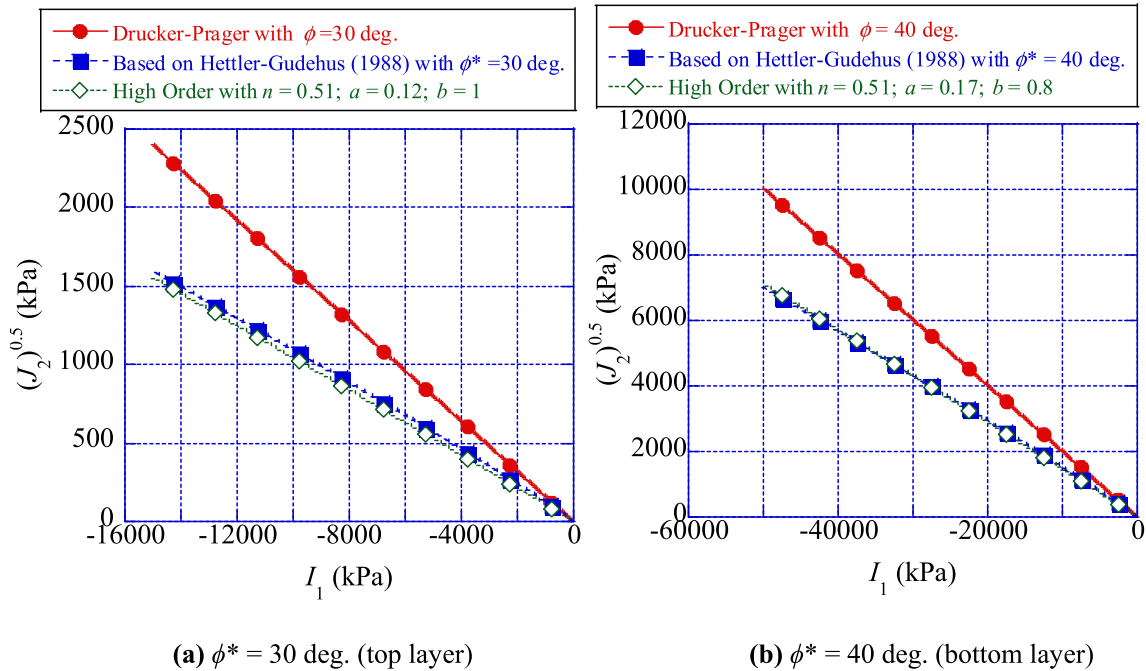
(a) $\phi*$ = 30 deg. (top layer)   **(b)** $\phi*$ = 40 deg. (bottom layer)

Fig. 16. Estimation of parameters *a*, *b* and *n* for ϕ soil.

(a) $\phi*$ = 20 deg., *c* = 45 kPa (top layer)   **(b)** $\phi*$ = 35 deg., *c* = 10 kPa (bottom layer)
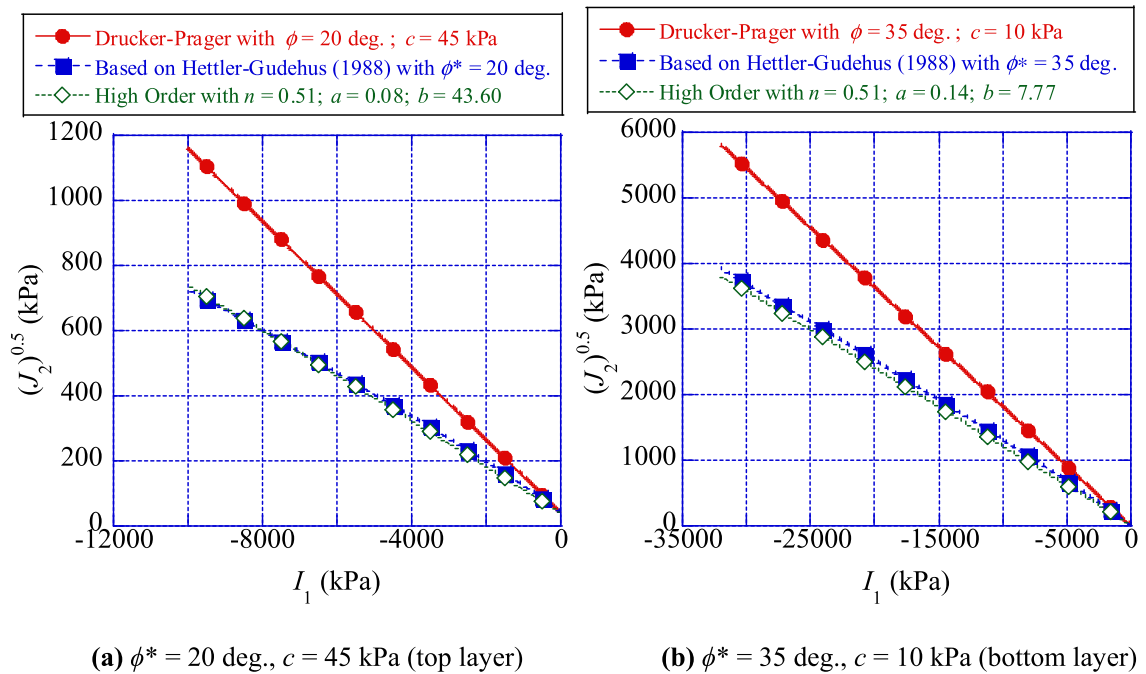
Fig. 17. Estimation of parameters *a*, *b* and *n* for *c-* ϕ soil.

Table 4
Coefficients for the soils used in the simulation.

Soil Type	Layer	ϕ (deg.)	*c* (kPa)	*n*	*a*	*b*
ϕ Soil	Top Layer	30	1	0.51	0.12	1.00
	Bottom ayer	40	1	0.51	0.17	0.80
c- ϕ Soil	Top Layer	20	45	0.51	0.08	43.60
	Bottom ayer	35	10	0.51	0.14	7.77

It can be concluded that RPFEM using D.P. can estimate the end bearing capacity of IESP in *c* soil.

In the case of the ϕ soil and *c-* ϕ soil, a good agreement is obtained between all the methods except the method of RPFEM using D.P.,which gives extremely high values of the end bearing capacity. From Fig. 24(b) and Fig. 24(c), it is clear that the D.P. yield function overestimates the end bearing capacity of IESP in the case of ϕ soil and
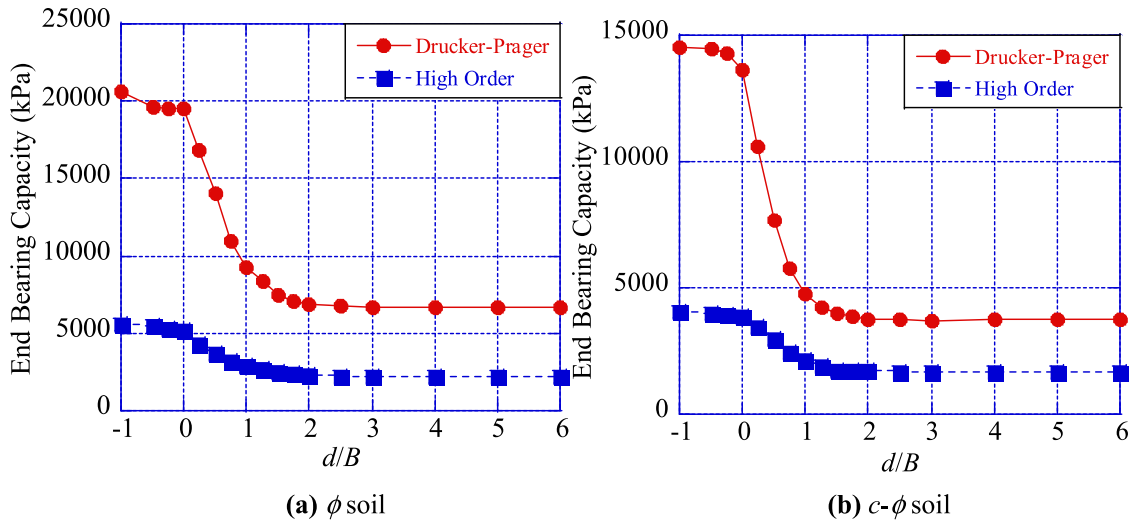
(a) ϕ soil   **(b)** c-ϕ soil

Fig. 18. Comparison of the end bearing capacities from D.P. and H.O. yield functions.

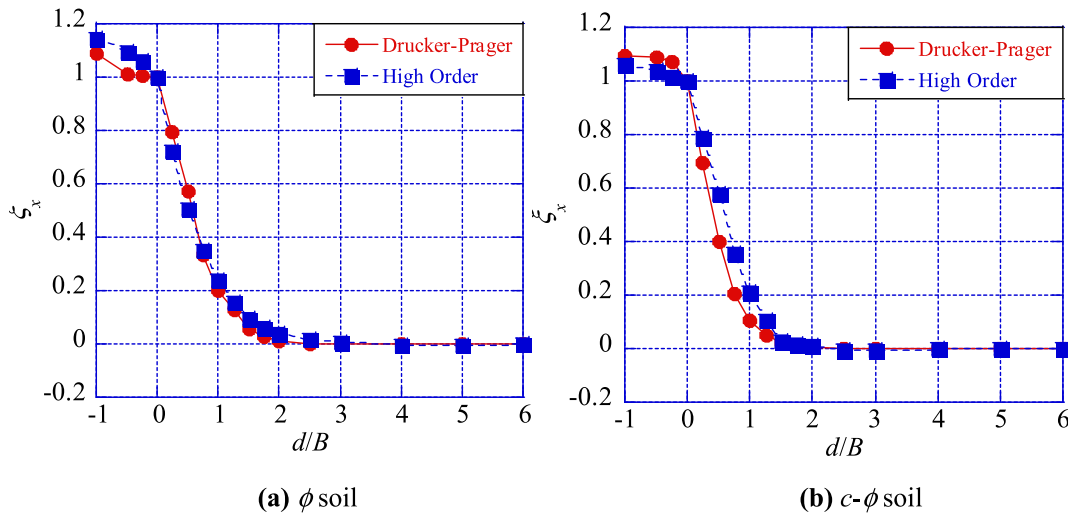**(a)** ϕ soil   **(b)** c-ϕ soil

Fig. 19. Normalized end bearing capacities from D.P. and H.O. yield functions.

c-ϕ soil. The High Order yield function gives an accurate estimation of the end bearing capacity of IESP in the case of ϕ soil and c-ϕ soil.

9.2. Comparison with Hyodo et al. (2020) and Ikeda et al. (2012) (Numerical and experimental method, respectively)

The proposed equation is compared with Hyodo et al. (2020). In the study by Hyodo et al. (2020), the bottom layer was very dense sand with relative density $D_r = 90\%$ and the top layer was changed from loose sand to medium sand and dense sand with relative densities $D_r = 45\%$, $D_r = 60\%$ and $D_r = 75\%$, respectively. The corresponding end bearing capacity q_{base} (=q_H) is about 475.67 kN and q_{nobase} (=q_s) are 251.34 kN, 319.47 kN and 392.15 kN for the case of sand in the upper layer has $D_r = 45\%$, $D_r = 60\%$ and $D_r = 70\%$ respectively, which correspond to $r = q_H/q_s = 1.89$, 1.49 and 1.21 respectively.

By using those ratios of r in Eq. (25) and Eq. (27), it was possible to obtain the corresponding ξ_x as a function of d/B. The comparison of the obtained ξ_x with those of Hyodo et al. (2020) (α) is shown in Fig. 25(a). There is good agreement between the two methods.

The ξ_x values were then used in Eq. (23) to obtain the corresponding q_x. Fig. 25(b) compares the ratio q_x/q_H, and there is good agreement between the two methods.

For more reliability, the laboratory loading tests with layered sand (Ikeda et al., 2012) are compared with the proposed formula. Here $q_s = 30.6$ kN and for $d/B = 0$, 0.5 and 1 the corresponding q_x are 103 kN (means $q_H = 103$ kN), 61.8 kN and 50 kN, respectively. Then the ratio $r = q_H/q_s = 3.37$. The black curves in Fig. 25(b) show the comparison of q_x/q_H, and that there is good agreement between the experimental method and the proposed equation.
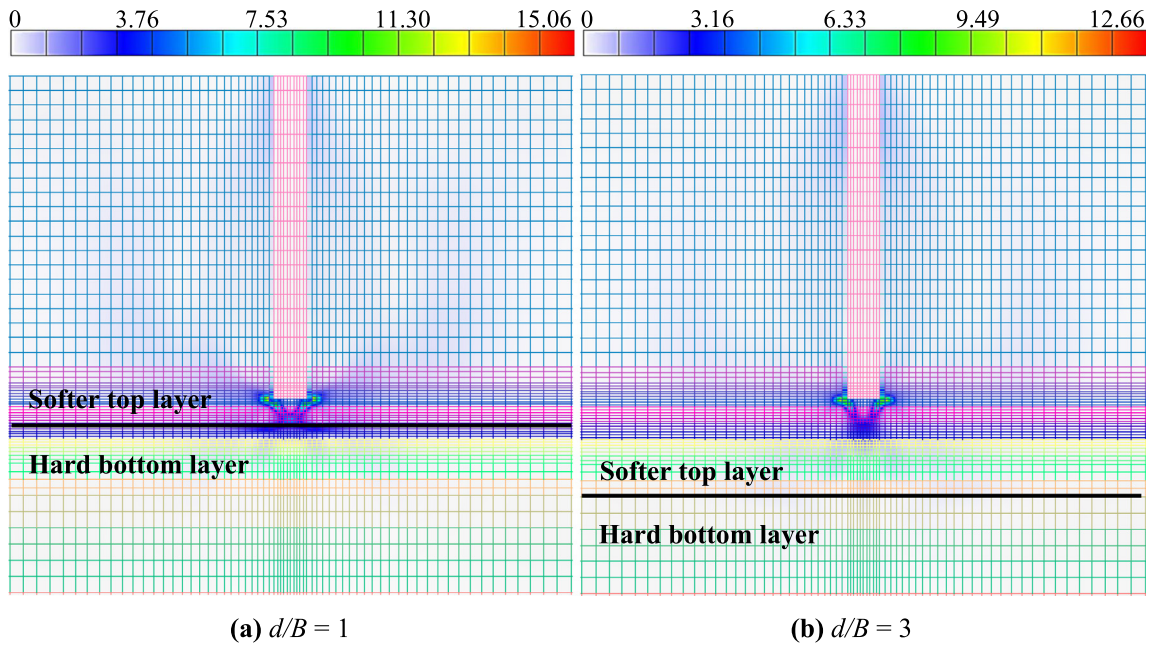
(a) *d/B* = 1   **(b)** *d/B* = 3

Fig. 20. Strain rate distribution from ϕ soil using the High-Order model yield function.

(a) *d/B* = 1   **(b)** *d/B* = 3
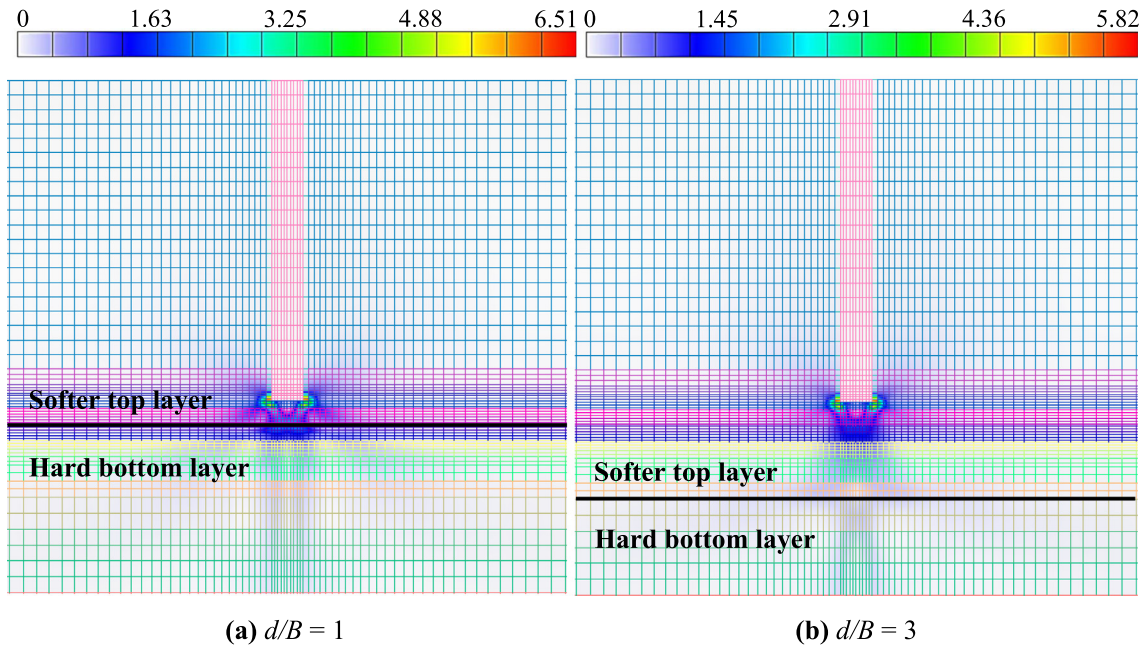
Fig. 21. Strain rate distribution from c-ϕ soil using the High-Order model yield function.

(a) $d/B = 1$ **(b)** $d/B = 3$
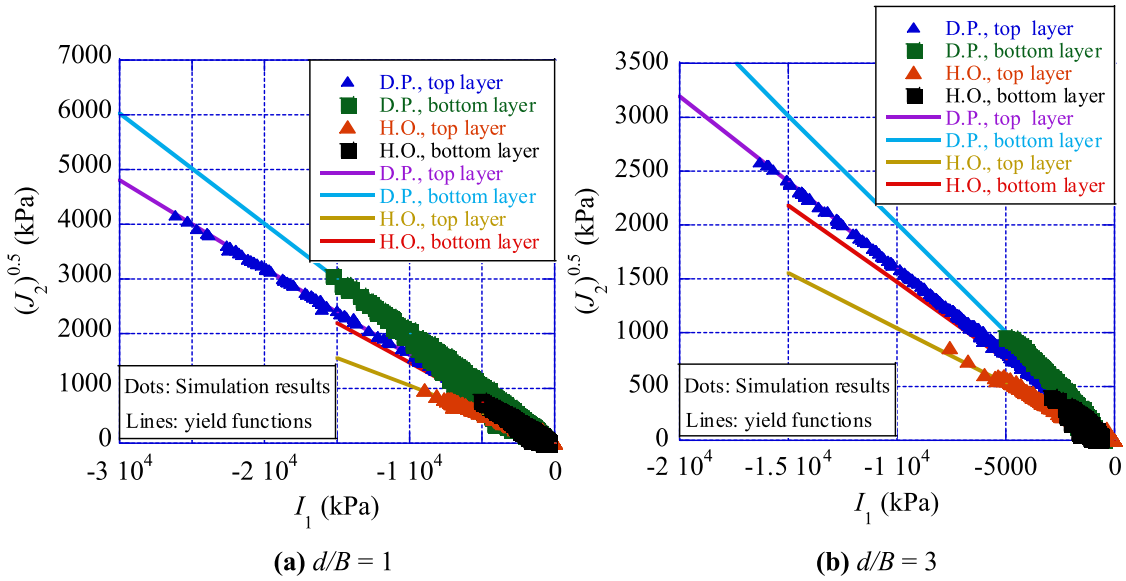
Fig. 22. Relationship between I_1 and $\sqrt{J_2}$ of ϕ soil.
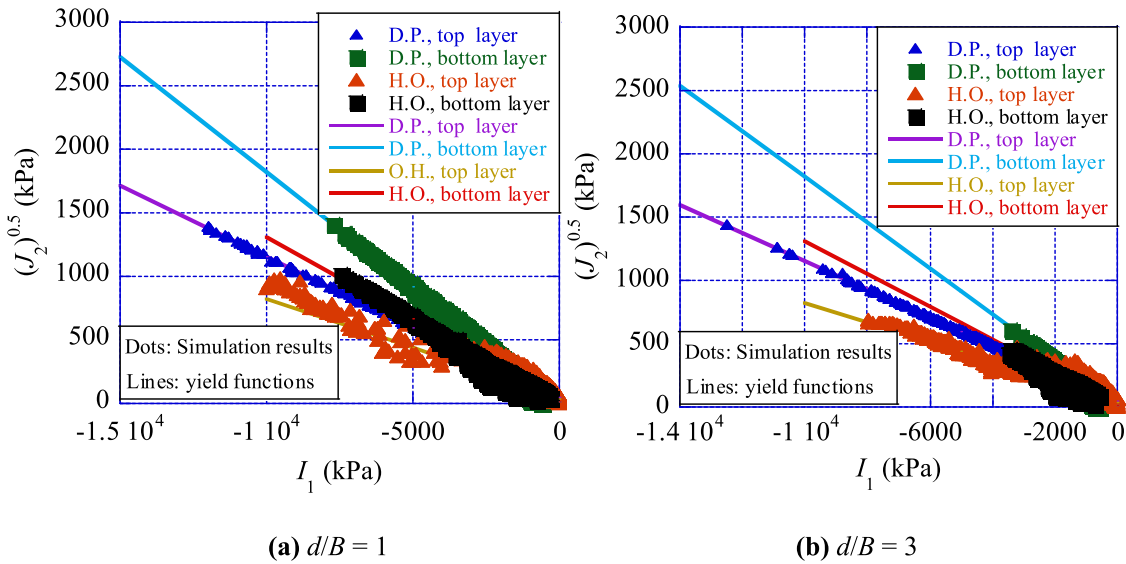

(a) $d/B = 1$ **(b)** $d/B = 3$

Fig. 23. Relationship between I_1 and $\sqrt{J_2}$ of c-ϕ soil.

Table 5
Equivalence between formulas.

Descriptions	Azam and Wang (1991)	Hyodo et al. (2020)	This study ((Eq. (22))
Formula	$q_0 = q_t + (q_b - q_t)\left[1 - m(H/B)\right]^2$	$q_{unreached} = \alpha q_{base} + (1-\alpha)q_{nobase}$	$q_x = \xi_x q_H + (1-\xi_x)q_s = \xi_x(q_H - q_s) + q_s$
End bearing capacity of IESP	q_0	$q_{unreached}$	q_x
End bearing capacity of completely end-supported pile (ESP) (when the pile reaches the bottom layer)	q_b	q_{base}	q_H
End bearing capacity of pile with no lower hard layer (no influence of the bottom layer)	q_t	q_{nobase}	q_s
Degradation factor	$\left[1 - m(H/B)\right]^2$	α	ξ_x

(a) *c* soils

(b) ϕ soils

(c) *c*-ϕ soils
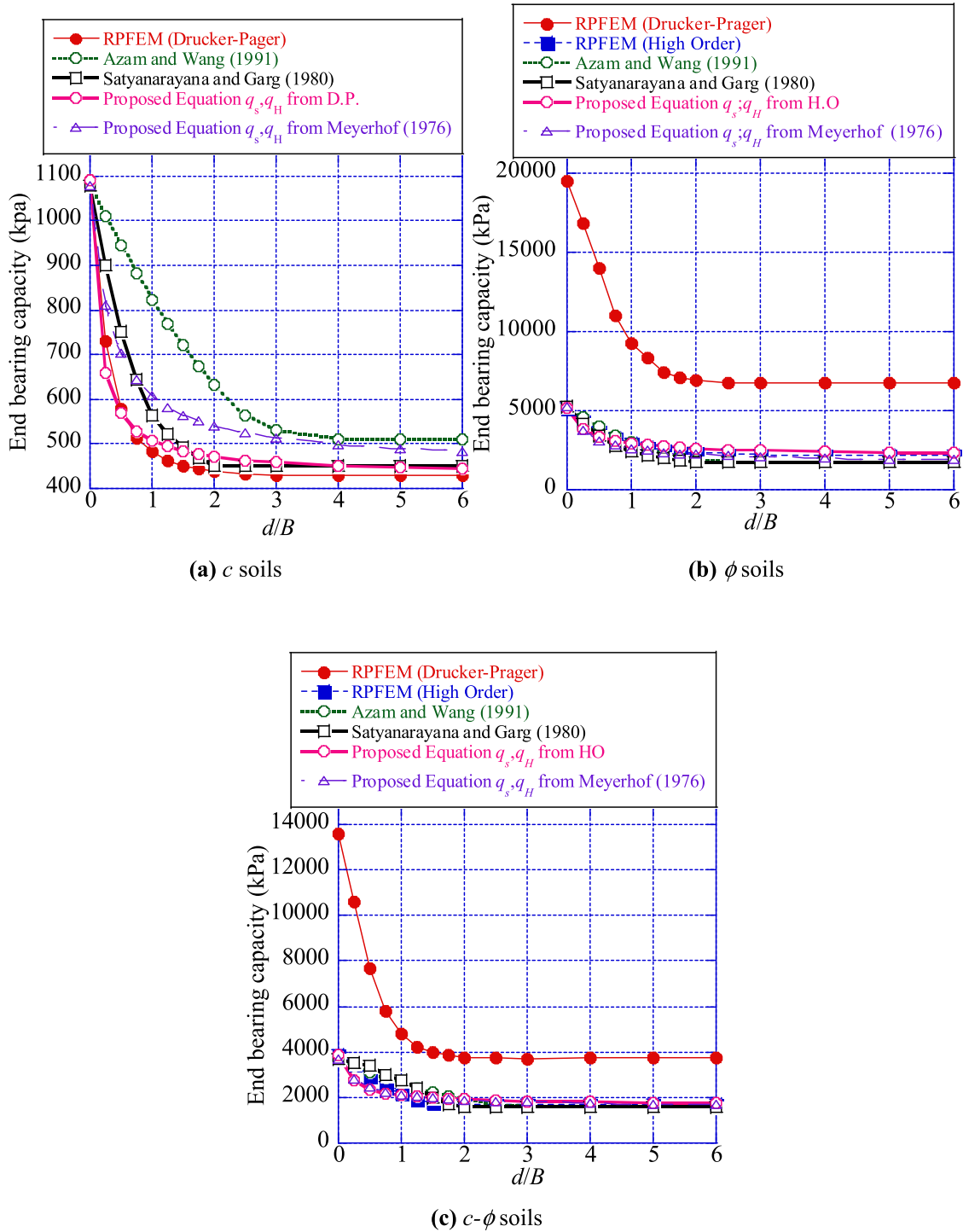
Fig. 24. Comparison with some analytical methods existing in the literature.

(a) Comparison of ξ_x
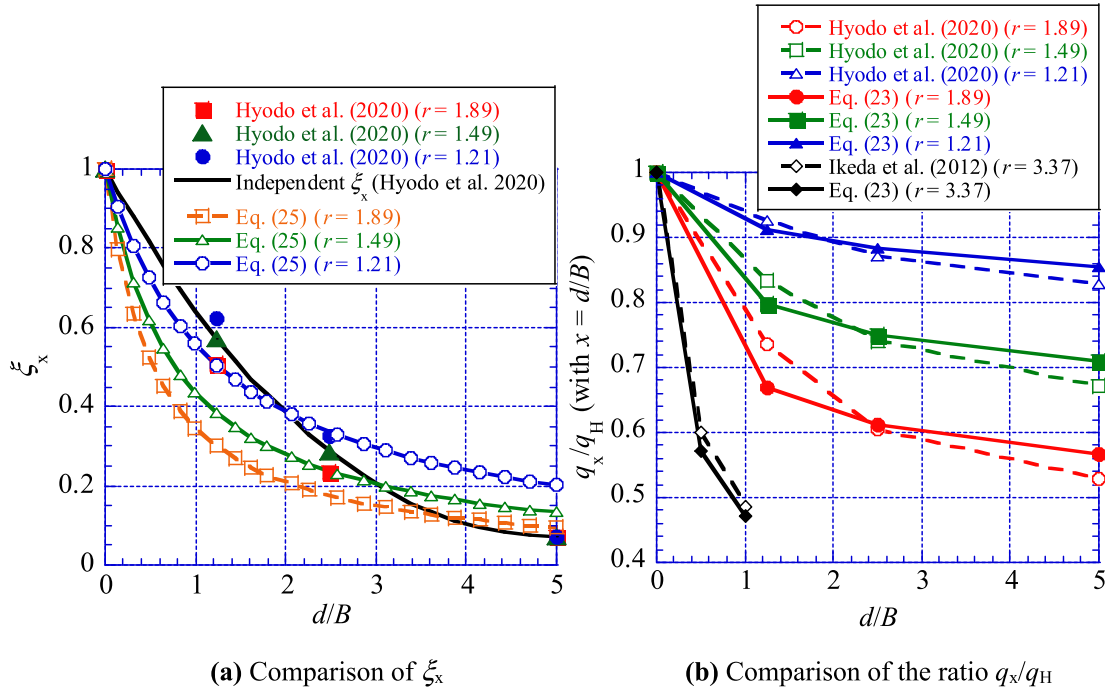
(b) Comparison of the ratio q_x/q_H

Fig. 25. Comparison with Hyodo et al. (2020) and Ikeda et al. (2012).

These comparisons verfy the accuracy and reliability of the proposed formula against past numerical and experimental results for ϕ soils. The comparison with analytical studies is sufficient to validate the proposed formula for c soils and c-ϕ soils.

10. Conclusions

In this study, a two-dimensional RPFEM analyss in the plain strain condition was carried out in order to estimate the end bearing capacity of an Incompletely end-supported single pile (IESP). Two yield functions were used, the Drucker-Prager yield function and the High Order yield function. Three types of soil were considered: c soil, ϕ soil and (c-ϕ soil). The influences of two parameters were investigated: the distance between the pile tip and the bottom layer normalized by the pile diameter (d/B), and the ratio r of the end bearing capacity of the pile on the bottom layer to that of the pile when the bottom layer has no influence. The main findings are as follows.

(1) The Drucker-Prager yield function gives reasonable results for c soil but is not suitable for ϕ soil and c-ϕ soils due to non-consideration of the influence of the confining pressure on the internal friction angle ϕ.

(2) New parameters of the High Order yield function are established to consider the non-linear shear strength property of soil against the confining pressure in ϕ

soil and c-ϕ soils. The validity of the established High Order yield was confirmed by comparing the results with those from existing literature. Therefore, a new yield function effective for estimating the end bearing capacity in ϕ soil and c-ϕ soil is established.

(3) Independent of the yield function (Drucker-Prager and High Order model), the end bearing capacity decreases when the pile goes far from the bottom layer and becomes constant from the distance of three times the pile diameter. The decrease of the end bearing capacity illustrates the degradation of the end bearing capacity.

(4) The degradation factor ξ_x of the end bearing capacity of IESP is independent of the yield function. However, ξ_x is affected by the bearing capacity ratio r and the soil type.

(5) An equation of the degradation factor ξ_x is established in this study as a function of the distance d/B, the end bearing capacity ratio r and the type of soil considered. Using ξ_x, a formula that gives an accurate estimation of the end bearing capacity of IESP is proposed. Its validity is confirmed by comparing the results with results from previous studies.

References

Azam, G., Wang, M.C., 1991. Bearing Capacity of Strip Footing Supported by Two-layer C-φ Soils. Washington, D. C: Transportation Research Record, Transportation Research Board No. 1331, pp. 56–66.

Berezantzev G., V., Yaroshenko A., V., 1962. Osobennosti deforminovania peschanych osnovanii pod fundamentami glubokogo zalozhenia. Osnovaniya I Fundamenty 4, 3–7.

Bishop, R.F., Hill, R. and Mott, N.F., 1945. The theory of indentation and hardness tests. In: Proceedings of the Physical Society, 57, 147–159.

Bowles, J.E., 1996. Foundations Analysis and Design. McGraw-Hill Publishing Company, New York.

Buisman S.K., A., 1935. De Weerstand van Paalpunten in Zand. De Ingenieur 50 (Bt. 25–28), 31–35.

Caquot, A., 1934. Equilibre des massifs à frottement interne. stabilité des terres, pulve´rulentes ou cohe´rentes. Gauthier-Villars, Paris.

Coyle, H.M., Castello, R.R., 1981. New design correlations for piles in sand ASCE. J. Geotech. Eng. Div. 107 (7), 965–986.

De Beer E., E., 1945. Etude des fondations sur pilotis et des fondations directes. Annales des Travaux Publics de Belqique 46, 1–78.

Du, N.L., Ohtsuka, S., Hoshina, T., Isobe, K., 2016. Discussion on size effect of footing in ultimate bearing capacity of sandy soil using rigid-plastic finite element method. Soils Found. 56 (1), 93–103.

Eslami, A., Fellenius, B.H., 1995. Toe bearing capacity of piles from cone penetration test (CPT) data. In: Proceedings of the International Symposium on Cone Penetration Testing, CPT'95, Linköping, Sweden. Swedish Geotechnical Institute, October 4–5, SGI Report 3-95, vol. 2, pp. 453–460.

Eslami, A., Fellenius, B.H., 1997. Pile capacity by direct CPT and CPTu methods applied to 102 case histories. Can. Geotech. J. 34 (6), 886–904.

Gunaratne, M., 2006. The foundation Engineering Handbook. Taylor and Francis, London.

Houlsby, G.T., Nuit, N.R.F. and Sweeney, M., 1994. End bearing capacity of piles in carbonate soil. In: Proceedings of the 13th International Conference on Soil Mechanics and Foundation Engineering, New Delhi, vol. 2, pp. 635–638.

Hettler, A., Gudehus, G., 1988. Influence of the foundation width on the ultimate bearing capacity factor. Soils Found. 28 (4), 81–92.

Hoshina, T., Ohtsuka, S., Isobe, K., 2011. Ultimate bearing capacity of ground by rigid-plastic finite element method taking account of stress-dependent non-linear strength property. J. Jpn. Soc. Civil Eng. Ser. A2 (Appl. Mech. (AM)) 68 (2), 327–336 (in Japanese).

Hyodo, J., Tamari, Y., Sone, A., Ozutsumi, O., Ichii, K., 2020. A simplified method to consider the pile of insufficient length to obtain the support from bearing stratum. J. Asian Arch. Build. Eng. 19 (6), 626–636. https://doi.org/10.1080/13467581.2020.1764847.

Ikeda, A., Tsutiya, T., Nagai, H., 2012. A new formula for the toe resistance of a helical screw pile considering the different load sharing bearing mechanism at the closed end and the helix. AIJ J. Technol. Des. 18 (40), 877–882.

Janbu, N., 1976. Static bearing capacity of friction piles. In: Proceedings of the 6th European Conference on Soil Mechanics and Foundation Engineering, vol. 1, no. 2, pp. 479–488.

Jáky, J., 1948. Pressure in silos. In Proceedings of the 2nd International Symposium on Soil Mechanics and Foundation Engineering (ICSMFE) 1, 103–107.

Meyerhof G., G., 1951. The ultimate bearing capacity of foundations. Géotechnique 2 (4), 301–332.

Meyerhof, G.G., 1963. Some recent research on the bearing capacity of foundations. Can. Geotech. J. 1 (1), 16–26.

Meyerhof, G.G., 1976. Bearing capacity and settlement of pile foundations ASCE. J. Geotech. Eng. Div. 102 (3), 195–228.

Pholkainuwatra, P., Eua-apiwatch, S., Yimsir, S., 2022. Experimental study of pile set-up of driven piles in Bangkok Clay. Eng. Appl. Sci. Res. 49 (1), 96–102.

Prandtl, L., 1920. Über die Härte plastischer Körper. In Nachrichten von der Königlichen Gesellschaft der Wissenschaften zu Göttingen. Mathematisch–physikalische Klasse aus dem Jahre, Berlin, pp. 74–85.

Prandtl, L., 1921. Uber die Eindringungsfestigkeit (Harte) plastischer Baustoffe und die Festigkeit von Schneiden. Z. Angew. Math. Mech. 1 (1), 15–20.

Reissner, H., 1924. Zum Erddruck problem. In: Biezeno, C., B.B., Burgers, J., M.M. (Eds.), In Proceedings of the 1st International Congress of Applied Mechanics. Delft, J. Waltman, jr., Delft, the Netherlands, pp. 295–311.

Satyanarayana, A.M., Garg, R.K., 1980. Bearing capacity of footings on layered c-φ soils ASCE. J. Geotech. Eng. Div. 106 (7), 819–824.

Skempton W., A., Yassin, A., Gibson R.E., M., 1953. Theorie del la force portante des pieux. Annales de l'Institut Technique du Batiment et des Travaux Publics, 63rd–64th., 6 l'Institut Technique du Batiment et des Travaux Publics, pp. 285–290.

Tamura, T., Kobayashi, S., Sumi, T., 1984. Limit analysis of soil structure by rigid-plastic finite element method. Soils Found. 24 (1), 34–42.

Tamura, T., Kobayashi, S., Sumi, T., 1987. Rigid plastic finite element method for frictional soil. Soils Found. 27 (3), 1–12.

Tatsuoka, F., Sakamoto, M., Kawamura, T., Fukushima, S., 1986. Strength and deformation characteristics of sand in plane strain compression at extremely low pressures. Soils Found. 26 (1), 65–84.

Teramoto, S., Kimura, M., Boonyatee, T., 2015. Parametric FEM analysis on mechanical behavior of Incompletely End-Supported Pile. Computer methods and recent advances in geomechanics-Oka; Murakami, Uzuoka and Kimoto (Eds.). London: Copyright Taylor and Francis Group, ISBN 978-1-138-00148-0.

Terzaghi, K., 1943. Theoretical Soil Mechanics. Chapman and Hall, London.

Veiskarami, M., Eslami, A., Kumar, J., 2011. End-bearing capacity of driven piles in sand using the stress characteristics method: analysis and implementation. Can. Geotech. J. 48, 1570–1586.

Vesić, A.S., 1967. Ultimate load and settlement of deep foundations in sand. In: Proceedings of the Symposium on Bearing Capacity and Settlement of Foundations. Durham, N.C, Duke University Series, vol. 5, no. 6, pp. 53–68.

Vesić, A.S., 1973. Analysis of ultimate loads of shallow foundations. J. Soil Mech. Found. Div. 99 (1), 45–76.

Vesić, A.S., 1977. Design of Pile Foundations. National Cooperative Highway Research Program, Synthesis of Practice No. 42, Transportation Research Board, Washington, DC, 68 pages.

Yasufuku, N., Hyde, A.F.L., 1995. Pile end-bearing capacity in crushable sands. Géotechnique 45 (4), 663–676.

Yasufuku, N., Ochiai, H., Ohno, S., 2001. End-Bearing Capacity of sand related to soil compressibility. Soils Found. 41 (4), 59–71.